NASA TECHNICAL NOTE

$c.1$

USE OF PHOTOIONIZATION
IN MEASURING VELOCITY PROFILE
OF FREE-STREAM FLOW IN LANGLEY
PILOT MODEL EXPANSION TUBE

by Wilfred J. Friesen

Langley Research Center
Langley Station, Hampton, Va.

USE OF PHOTOIONIZATION IN

MEASURING VELOCITY PROFILE OF FREE-STREAM FLOW IN

LANGLEY PILOT MODEL EXPANSION TUBE

By Wilfred J. Friesen

Langley Research Center
Langley Station, Hampton, Va.

NATIONAL AERONAUTICS AND SPACE ADMINISTRATION

USE OF PHOTOIONIZATION IN
MEASURING VELOCITY PROFILE OF FREE-STREAM FLOW IN
LANGLEY PILOT MODEL EXPANSION TUBE

By Wilfred J. Friesen
Langley Research Center

SUMMARY

Free-stream velocity profile measurements have been made of expansion-tube flows for flow-core velocities of the order of 6300 m/sec, for flow-core densities ρ/ρ_0 (where ρ is the gas density and ρ_0 is the gas density at standard conditions) from 3×10^{-4} to 2×10^{-3}, and over flow time intervals of about 150 μsec. The method of measurement was based on identifying a region of the flowing test gas by photoionization and, after a delay of a few microseconds, photographing the displaced position of the region by the light emitted when an electrical current was passed through it. The main conclusions reached are that there is a flow core with a radius between 50 and 60 percent of the tube radius, in which the velocity is uniform to within 5 percent, and that the method of measurement is a useful technique for obtaining velocity profiles within this range of test-gas density.

INTRODUCTION

The purpose of the present investigation was to measure the velocity profile of the flow in the Langley pilot model expansion tube. The development of a method of making the measurement was also a necessary part of this investigation. Some of the basic performance characteristics of the 9.55-cm-diameter expansion tube and a detailed description of the tube and the nomenclature used herein have been reported in reference 1.

Flow-core velocities of the order of 6300 m/sec and flow-core densities of the order of $\rho/\rho_0 = 1 \times 10^{-3}$ were the expected flow properties in the expansion tube.

One of the basic problems involved in making a direct measurement is identifying a region of the transparent and presumably homogeneous gas. The identification of a region of the gas generally requires the addition of energy to the region, and this energy addition should introduce a minimum disturbance to the average kinetic energy of the molecules of the flowing gas.

One approach to identifying the motion of the gas, which was abandoned, involved observing the drift of a cylindrical shock wave in the gas. The technique for producing the shock wave was to be a long spark struck across the flow diameter. This shock wave was to be observed with a schlieren system. This approach was abandoned after preliminary experiments indicated that, for the conditions to be encountered in the expansion-tube flow, a long spark could not be obtained reliably and the schlieren technique was not sensitive enough to observe the shock wave at the low densities.

The technique presented in this paper is similar to the approach reported in reference 2 except for the use of a different means to identify the flow region. In reference 2 a region of the gas flow, in a wind tunnel, was identified by the residual ionization produced by a long spark struck between electrodes in the gas. The initial position of the region was photographed by the light from the spark. After a suitable time delay the final position of the region was photographed by the light produced when a second current pulse was passed through the now conducting region.

In the present paper a region of the gas was identified by partial ionization with the use of an ionizing source external to the flow region. Some of the advantages of this technique are:

(1) The initial position and diameter of the partially ionized region can be well defined independent of the electrical characteristics of the flowing gas.

(2) The disturbance to the gas flow should be reduced since the initial position of the region is determined geometrically and additional energy need not be added to the region in order to observe its initial position.

(3) The diameter of the region can be controlled.

The final position of the displaced region was observed by the light produced by a current pulse through the ionized region, the same technique that was used in reference 2.

A pulsed electron beam was used in the first attempts at ionizing a region of the gas by means of an external source. The electron source produced a focused beam with an energy of 20 000 electron volts, a current of 3×10^{-3} ampere, and a pulse duration of 1×10^{-7} second. For static (no-flow) conditions in the test chamber of the expansion tube, at gas densities to be encountered in the flow, this source produced enough ionization to be detected by the current pulse. When this source was tested in the expansion-tube flow, insufficient ionization was produced compared with the ionization present in the wall boundary flow to be detected by the current pulse. The failure of these attempts to use an electron source appeared to be due to insufficient beam current. Since a means of increasing the electron beam current was not readily available, these attempts were discontinued.

The ionizing source used in the experiments presented herein was a pulsed beam of ultraviolet light. After a time delay the final position of the ionized column was made visible by passing a current pulse through the displaced column which was then photographed.

The work presented in this report represents the first direct measurements of the velocity profile of the Langley pilot model expansion tube flow and also demonstrates the feasibility of using an external ionizing source for the study of low-density gas flows.

SYMBOLS

D	diameter of expansion tube, 0.0955 meter
F	local diameter of the cone of full illumination of the ultraviolet light source
p_t	pitot pressure
p_1	initial pressure in intermediate (test-gas) chamber
p_{10}	initial pressure in acceleration chamber
R	tube radius
Δt_1	time interval between passage of helium-air interface and velocity measurement
Δt_2	time interval between ionization and detection of a region of the gas flow
u	flow velocity
u_c	average flow-core velocity of a single profile
u_l	limiting velocity of an unsteady expansion wave
Δx	displacement of ionized column parallel to tube axis
y	radial position with respect to tube axis
α	absorption coefficient at standard density

$\delta_{0.95}$ boundary-layer thickness, measured from tube wall to point where velocity is 95 percent of core velocity

ρ gas density

ρ_o gas density at standard conditions (1.293 kg/m^3 for air)

DESCRIPTION OF APPARATUS

A static test chamber was used in addition to static tests in the expansion-tube test section for development of the velocity measuring technique. The purpose of the static tests was to determine some of the properties of the ultraviolet (uv) source and operating parameters for the source and detector circuitry. No attempt was made in these static tests to simulate the density distribution which would be present under flow conditions. Thus the windowless uv light source, for example, was operated in air at the test-chamber density during static tests but was operated in helium at a much lower density during an expansion-tube run.

The velocity profile measurements were conducted in the free stream of the test section of the 9.55-cm inside-diameter Langley pilot model expansion tube. Figures 1 and 2 schematically show the arrangement of the primary apparatus about the test section. The essential components are the uv light source, detector electrodes, camera, time-interval detector, and flow-events detectors.

Pulsed uv Light Source

Figure 2 shows the main details of the windowless light source. The light is produced from an electrical discharge in a 0.076-cm-diameter, 1.9-cm-long pyrex capillary tube which was open to the test section at one end. The 0.025-cm-diameter pointed tungsten electrode was pulsed negative to approximately 30 000 volts for a duration of 0.1 μsec. The collimating tube serves as the electrostatic shielding and is operated at ground potential. The pulse generator consisted of a coaxial cable in which the energy was stored. This cable was charged to 40 000 volts and was discharged through the source. The stored energy in the pulser was approximately 4 joules. The uv-source pulser circuit is shown in figure 3(a) and is similar to that described in reference 3.

Detector Electrode

The detector electrode consisted of a 0.025-cm-diameter tungsten wire recessed 1.27 cm from the end of a plastic tube and is schematically shown in figure 2. The pulse generator for the detector electrode was similar to the pulse generator for the uv light

4

source and is shown in figure 3(b). The circuit produced approximately a 4000-volt pulse of 0.1-μsec duration at the detector electrode.

Camera

A biplanar diode was used as the electronic shutter for the camera. A shutter was required because considerable light is associated with portions of the flow following the testing region of the flow in the expansion-tube cycle. The front and relay optics of the camera were f/2 and f/1.9, respectively. A 1-μsec shutter-open time was used. The picture was photographed on high-speed film.

Time-Interval Detector

The time interval between ionization of the gas by the uv light and the illumination of the displaced ionization region was obtained from a photomultiplier signal. The photomultiplier viewed the visible light scattered up the plastic detector electrode from the uv light source, which was in line with it, and from the illuminated region in the test chamber. The signal from this photomultiplier was displayed on an oscilloscope along with a 1-μsec timing calibration signal on the same oscilloscope channel.

Flow-Events Detectors

The arrival of the test air at the test section was detected by two detectors. One detector was a photomultiplier which viewed the end of the expansion tube, where the flow entered the test section. This detector responded to a low-level light signal associated with the helium-air interface. The second detector was a thin-film heat-transfer gage located in the wall of the expansion tube approximately 26 cm upstream of the test section. This detector responded to the helium shock wave which immediately preceded the arrival of the test air. These detectors provided the reference time for determining the position of the velocity measurement in the test-air flow and were used for the initiation of the sequence of events in a velocity measurement.

BASIS FOR VELOCITY MEASUREMENTS

The velocity measurements were based on at least two assumptions:

1. A region of the gas could be identified from the surrounding gas by partial ionization of the gas in the region by means of ultraviolet light from an electrical discharge in a capillary.

2. The position of the partially ionized region could be detected from the light emitted when an electrical current was passed through the region.

To assess the first assumption, tests were conducted in the static test chamber and the results are presented next under the heading "Identification." To assess the second assumption, tests were conducted during the course of the velocity measurements in the expansion tube and the results are presented in the "Discussion of Results" section under the heading "Detection."

Identification

Ionization produced by uv light.- A windowless parallel-plate ionization chamber was placed at the center of the static test chamber. The ionization chamber was located 16.5 cm from the uv source. Figure 4 shows the variation of the ion density observed at the center of the static chamber with the static chamber density for a typical source. The ion density was estimated from the measured ionization and the geometry of the system.

Also shown in figure 4 is the relative response of a photomultiplier which viewed a low-level light which was emitted from the air in the light path of the source. By the use of a bright visible light source it was shown that the response of the photomultiplier was not due to the scattering of visible light emitted by the uv source. The light viewed by the photomultiplier was assumed to be associated with the ionization of the air in the chamber.

Diameter of ionized region.- Figure 5 shows the photomultiplier response as the region in the center of the chamber was scanned perpendicular to the ionizing beam. The solid curves indicate those data for which a small magnet was placed near the source to deflect electrons emitted by the source. The curves are normalized, for the sake of comparison, to the peak values occurring with the magnetic field present. The curves show that the width of the excited region is essentially independent of the chamber density and is in agreement with the estimated cone of full illumination of the source. Figure 5 shows that electrons from the source have the greatest effect at the lower densities.

Attenuation of ionizing beam.- Figure 6 shows plots of the relative photomultiplier response for positions along the uv beam axis for several chamber densities ρ/ρ_0. The height of the scanning slit was made large enough to insure that the entire local beam diameter was included for all positions along the beam axis. The individual curves in figure 6 tend to indicate an exponential behavior which would be in agreement with photon absorption.

Figure 7 shows a plot of the effective absorption coefficient referred to standard density (α) for the ionizing radiation. These results were estimated from the slopes of the curves of figure 6 for each chamber density. The values of α shown in figure 7 are of the same order of magnitude as the values of the monoenergetic photoionization coefficients of nitrogen and oxygen in reference 4. In figure 7 α tends to increase with a decrease in chamber density. Since α is not constant with changes in chamber density,

the uv source cannot be approximated by a monochromatic source over the range of chamber densities shown.

Duration of ionization time interval.- The duration of the low-level light from the ionization was about 10^{-7} second, which corresponded to the pulse duration of the properly terminated pulser. The visible light from the uv light source had a longer duration than the light from the ionized region and the intensity of this visible light increased with an increase in chamber density.

EXPANSION-TUBE TEST CONDITIONS

The driver chamber was pressurized with room-temperature hydrogen to a self-burst pressure of about 9.7 MN/m^2.

The test-gas chamber was filled with air or nitrogen to a pressure of 22 torr (2930 N/m^2) with the exception of three runs at 100 torr (13 300 N/m^2).

The acceleration chamber was filled with helium (He). Three main pressures were used in order to obtain data over a range of flow-core densities. Data were also taken for at least three different times behind the He-(air or nitrogen) interface for each initial condition p_{10}. Since no observable differences were noted between operation with air or nitrogen, the He-(air or nitrogen) interface will be called the He-air interface. Each determination of the velocity profile required a separate expansion-tube run and several test conditions were repeated in order to check the reproducibility of the results. The number of runs made for each condition reported in this paper is given in table 1.

TABLE 1.- EXPANSION-TUBE TEST CONDITIONS

p_{10}		Δt_1, μsec	Number of runs
torr	N/m^2		
$p_1 = 22$ torr $= 2930$ N/m^2; $u_l = 8595$ m/sec			
0.0047	0.63	53	1
.010	1.3	60	6
		109	2
		227	1
.046	6.1	26	2
		54	9
		155	2
.090	12	24	2
		52	3
		150	2
$p_1 = 100$ torr $= 13\ 300$ N/m^2; $u_l = 6550$ m/sec			
0.009	1.2	52	1
.046	6.1		
.091	12.1		

PROCEDURE

The velocity measurements were made in the air or nitrogen flow following the He-air interface. The sequence of events of a velocity measurement was triggered from the arrival of the He-air interface at the test section either by the photomultiplier viewing the entrance to the test section or the heat transfer gage located approximately 26 cm upstream of the test section.

Figure 8 is a schematic diagram of the time sequence of events which followed the arrival of the interface at the test section. After a delay Δt_1 which was varied over a range of 20 to 150 μsec, a column of the test air was ionized by pulsing the uv light source. After a delay Δt_2 of about 2 μsec, the displaced column was illuminated by pulsing the detector electrode. The camera shutter was synchronized with the detector pulse so that the illuminated displaced column was photographed.

The time behind the He-air interface at which the velocity measurement was made (Δt_1) was obtained from the oscilloscope display of the photomultiplier which viewed the entrance to the test section. The time interval between the ionization and detection of the ionized column (Δt_2) was obtained from the oscilloscope display of the photomultiplier which viewed the visible light scattered up the plastic detecting electrode.

The displacement of the ionized column Δx at various positions across the flow core during the time interval Δt_2 was obtained from microdensitometer scans of the photograph. The electrodes were illuminated and photographed prior to the run on the same film on which the data were recorded. The position of the electrodes on each film was used for both the reference position and scale-factor calibration for each run. The initial position of the ionized column with respect to the electrodes was obtained from scans of photographs taken under static conditions on a separate film.

Samples of the data for an expansion-tube run are shown in figures 9, 10, and 11.

ACCURACY AND PRECISION

The overall accuracy of the velocity determined depends directly on the accuracy of the measurements of Δx and Δt_2. The accuracy of the profile of velocity determined depends only on the accuracy of the measurement of Δx since the time interval Δt_2 is presumed to be common to all elements of the flow. The time behind the He-air interface at which the velocity was measured was defined to about ± 5 μsec.

Uncertainties in Δx

Some of the quantities which would affect the accuracy of Δx are uncertainties in the film and densitometer-chart scale factors, in the location of the center of the luminous

region, and in the correction for the beam alinement. The compounding of these uncertainties leads to an estimated precision in Δx of about ±1 percent.

Scale factors.- The positions of the electrodes which appeared on the film were used to obtain the scale factor for relating the position of the displaced column on the densitometer scan chart to the position of the column in the test section. The distance between electrodes was measured to about ±0.1 percent. A scale factor was determined for each run in order to minimize the effects of possible changes in film dimensions due to processing and atmospheric conditions. An upper bound for uncertainties due to the dimensional instability of the film was estimated from the magnification obtained as the ratio of the estimated distance between the electrodes on the film compared with the measured distance between the electrodes in the test section. The standard deviation from the mean magnification for 28 runs in which the camera position remained the same was ±0.28 percent. The standard deviation from the mean overall scale factor for relating position on the densitometer chart to position in the test section for the same 28 runs was ±0.48 percent.

Location of center of luminous region.- The reproducibility of locating the center of the luminous region was tested by 10 repeated scans of the films from four runs. The standard deviation was ±0.0064 cm for points in the core of the flow and increased to ±0.023 cm in the boundary flow. The standard deviation for the entire group of 40 comparisons was ±0.015 cm. The larger deviation obtained for values in the boundary flow is due in part to the reduced brightness of the column and a diffuse luminous background in the boundary layer. The error of the measurements due to uncertainties in locating the center of the region was about ±0.5 percent in the flow core and varied to about ±5 percent in the boundary flow. The line-pair resolution specified by the manufacturer of the camera system for the magnification used was 0.023 cm or better.

Beam-alinement correction.- A correction was applied for the alinement of the ionizing beam. This correction was obtained for each setting of the electrodes from a photograph of the luminous region taken under static conditions in the test chamber of the expansion tube. The range of the applied correction was from 0.010 cm to 0.076 cm, ±0.008 cm for positions near the center of the flow.

Uncertainties in Δt_2

Some of the factors which contribute to uncertainties in Δt_2 are uncertainties in the measurement of the time interval on the oscilloscope record, calibration of the oscilloscope record, pulse shape, and time delays.

Measurement of time interval.- The reproducibility of measuring the time interval Δt_2 between pulses on the oscilloscope record was estimated from 40 measurements to be ±0.005 μsec. The 40 measurements were comprised of four repeated measurements

on the records of 10 runs. The error in Δt_2 due to reading the record for a typical time interval (2 μsec) is then ±0.25 percent.

Calibration.- A calibration of the oscilloscope record while recording the data on each run was provided by a 1-μsec time marker which was superimposed on the signal input of the oscilloscope. An upper bound for the precision of the calibration factor of ±0.4 percent was estimated from the standard deviation from the mean of the calibration factors of 28 runs.

Pulse shape.- The time interval Δt_2 was measured between two pulses which were not identical in shape. The shape of the light pulse from the detected region of the gas as observed by the time-interval detector agreed with the shape of the electrical pulse from the detector pulser. The light pulse observed by the time-interval detector and used for indicating the ionization of the gas was produced by the visible light from the uv light source with the possibility of some fluorescence of the detector electrode plastic, since the optical path to the photomultiplier was opaque to the ionizing radiation. This pulse has a slightly larger rise time and a longer decay than the detector pulse. The light from air excited by the ionizing radiation was found to have a pulse shape in agreement with the electrical pulse of the uv-light-source pulser and similar to the detector pulse. The time interval Δt_2 was taken as the time interval between the initial rise of the two pulses, and the rise time of the ionizing pulse was assumed to be the same as the rise time of the detector pulse. If the time interval had been assumed to be the interval between peak values of the pulses displayed, the time interval would have decreased about 0.07 μsec; for a 2-μsec time interval, this assumption would have decreased Δt_2 by about 4 percent.

Time delays.- The source light pulse and the detector light pulse were viewed by the same photomultiplier and displayed on the same oscilloscope channel so that the optical and electronic time delays were the same for both light pulses.

DISCUSSION OF RESULTS

Detection

Criterion for valid luminosity.- An examination of the photographs shown in figure 11 shows a diffuse background luminosity, which appears to be associated with the boundary-layer region of the flow, and also a brighter luminous path between the source and detector electrodes that is not symmetrical about the expansion-tube axis. An interchange in the positions of the two electrodes showed that the nonsymmetry was associated with the positions of the electrodes and was not due to a lack of symmetry in the flow about the tube axis.

The criterion used to determine which luminous regions correspond to the displaced ionized region in the flowing gas was that the flow velocity estimated for a point in the flow must be independent of the displacement Δx and the elapsed time interval Δt_2. Several expansion-tube runs were made for two conditions p_{10} in which the time interval between ionization and detection Δt_2 was varied. The results of these runs are plotted in figure 12 with Δt_2 as a parameter. In these figures the displacement as a function of position across the tube diameter is shown and also the velocity computed for each position is plotted.

Figure 12 shows that in the flow region from $y/R = -1.2$ (detector electrode) to $y/R = 0$ the displacements of the luminous region are in agreement with the criterion of validity. Figure 12 also shows that in the flow region from $y/R = 1.2$ (source electrode) toward $y/R = 0$ the displacements of the luminosity are not in agreement with the criterion of validity and are therefore not associated directly with the motion of the flow.

Extraneous luminosity.- The nature of the luminosity near the source electrode was investigated primarily in terms of its possible effect on a velocity measurement, and its cause is not really understood. The possibility that the luminous region was due to particles or a jet of gas from the capillary discharge was tested by moving the source farther from the axis of the expansion tube and placing an electrode with an aperture at the same position as the original end of the source electrode. This displacement of the source caused a reduction in the uv-light intensity in the test region but the penetration of the luminous region was the same as for the closer position of the source. This effect is not consistent with the increased transit time required for particles or a jet of gas. Some of the phenomena observed during these experiments were that (1) the luminous region extends further into the flow for a decrease in central density, and (2) the region always appears to be attached to or originates at the hole of the source electrode. In a few cases there was a limited region in the flow where the two luminous regions were observed to overlap.

These observations are consistent with a model in which photoelectrons are emitted at the wall of the collimating hole in the source electrode by visible light from the capillary discharge and are accelerated into the gas flow by the electric field when the detecting pulse is applied. Thereby a preferred discharge path in this region of the flow is provided. This speculation is introduced here primarily to indicate the possibility that the mechanism by which this luminous region is produced may be initiated during the detecting pulse and would not therefore influence the flowing gas during a velocity measurement.

Diameter of detected region.- Measurements of the diameters of the detected luminous column for static conditions are compared with the local diameters of the cone of full illumination in figure 13. The diameters were obtained from densitometer scans of

the photographs with the assumption that the column was uniformly luminous across any diameter. As a general trend, these curves lie parallel to the dashed-line representing the diameter estimated for the cone of full illumination of the uv light, with departures in the vicinity of the electrodes.

Figure 13 shows an increase in the diameters with an increase in the delay time Δt_2 for the lower densities. The diameters at the low densities appear to converge to the same value in figure 13(b).

In figure 14 the diameters of the luminous column for a position near the center of the column are compared for both flow and static conditions. This comparison shows results for a range of densities and for two delay times between ionization and detection. There appears to be a significant difference in the results for the static and flow conditions. The diameters obtained for flow conditions appear to be in fair agreement with the diameter of the cone of full illumination. The correction for motion shown in figure 14 was estimated to account for the blurring due to the finite ionization and detection time intervals of about 10^{-7} second each. The diameters obtained for the static conditions increase with decreasing density to about two times the diameter of the cone of full illumination. With the exception of the highest density condition, the differences between the static diameters and the diameter of the cone of full illumination are about an order of magnitude larger than the differences between the diameter after 2 μsec of diffusion of ions from the ionized column, as estimated by the method of reference 5, and the diameter of the cone of full illumination.

The photographs obtained under flow conditions are much dimmer than those obtained for static conditions. An estimate of the magnitude of the correction to the observed diameters due to nonlinearity of film density with exposure is beyond the scope of these measurements but would be in a direction to bring the measured static and flow diameters into closer agreement.

From these measurements, only a qualitative estimate of the diameter of the ionized column can be inferred from the luminosity produced by passing a current pulse through the ionized column.

Limitations of the Method

In order to make a velocity profile measurement, a photograph of the displaced luminous detected column was required. Obtaining a useful photograph will be used as the working definition of a successful measurement. In general the photographs obtained for the velocity profile measurements were dim as compared with photographs obtained for static conditions.

The electronic shutter used in the camera reduced the effective intensity at the film by about a factor of 10. Without this loss in photographic sensitivity the range of density for successful measurements is estimated to be increased by about a factor of 2.

Density.- Successful measurements were made over a range of flow-core densities ρ/ρ_0 of 3×10^{-4} to 2×10^{-3}. The density $\rho/\rho_0 = 3 \times 10^{-4}$ was the lowest density for which a measurement was attempted. The photograph obtained was dimmer than for mid-range densities. Attempts were also made to make measurements at higher estimated flow-core densities of $\rho/\rho_0 = 4 \times 10^{-3}$ and $\rho/\rho_0 = 8 \times 10^{-3}$. For $\rho/\rho_0 = 4 \times 10^{-3}$ only a portion of the ionized region near the center of the flow core was detected, and for $\rho/\rho_0 = 8 \times 10^{-3}$ the attempts were unsuccessful. The limited density range for the method may be expected from the variation of the ionization with density shown in figures 4 and 6.

Distance between detector electrode and uv source.- The distance between the detector electrode and the capillary source was increased to 1.35 times the distance used during the usual measurements. This change was made while keeping constant the distance from the detector electrode to source collimating hole and the solid angle subtended by the uv beam. Very dim photographs were obtained for several runs with this configuration. These results suggest that reduction in ionization density may set a limit to the distance between the uv source and detector electrode.

Delay between ionization and detection Δt_2.- For flow conditions, successful measurements were obtained for delays between ionization and detection up to 2.4 μsec. For static conditions, delays up to 10 μsec produced successful photographs. Since the flow velocities that were encountered in these measurements were all of similar magnitude, the results do not permit a determination of whether the limitation is primarily a function of time or displacement of the ionized column or both.

Time behind He-air interface Δt_1.- A limit to the minimum time behind the He-air interface for which a successful measurement could be made was observed. This limitation appears to be sensitive to p_{10} or density. Three attempts to obtain a measurement were unsuccessful for $\Delta t_1 = 20 \mu$sec, with $p_{10} = 0.01$ torr $= 1.3$ N/m^2. Under static conditions with the chamber filled with He the detector pulse did not illuminate the path of the uv beam. The reason may be the much higher ionization potential of He as compared with nitrogen and oxygen. A possibility exists that some time interval following the passage of the He-air interface is required to flush the initial He from the vicinity of the detecting electrode. The sensitivity of the limitation to p_{10} may result from the combined effects of decrease in density and increase in boundary-layer thickness as p_{10} decreased.

Extraneous luminosity near source electrode.- The luminous region near the source electrode limits the observation of the ionized column. The distance to which this

luminosity extends into the flow (see figs. 11 and 12) depends on the density and might limit measurements at low densities.

Velocity Profile Measurements

The results of the velocity and velocity profile measurements are presented in figures 15 to 20. The results presented in these figures were obtained from data in the region from the center line of the flow to the vicinity of the detector electrode ($y/R = 0$ to $y/R = -1.1$). The reproducibility of a repeated-run condition is presented in figure 15.

All the results presented in figures 16 to 20 are in terms of two main parameters — the initial He pressure in the acceleration chamber of the expansion tube p_{10} and the time after the passage of the He-air interface Δt_1. The deviation represented by a bar is the estimated standard deviation of the mean and is indicated except where the size of the plotting symbol is larger than the deviation. No uncertainty is indicated for those results which were obtained from a single run.

The velocities which are presented at $\Delta t_1 = 0$ in figures 19(a) and 20(a) are the He-air interface velocities obtained from microwave data (ref. 1), since attempts to measure the velocity close to the interface were unsuccessful.

The arrival of the expansion fan at the test section, which is shown in figures 18, 19, and 20, was obtained from data from static-pressure gages located along the expansion tube.

Two velocities, u_c and u_l, were used in normalizing the results for comparison. The velocity u_c is the average flow-core velocity. The velocity u_l is the limiting velocity obtainable by expanding the gas in the intermediate (test-gas) chamber to nearly zero pressure by an unsteady expansion wave. This term is defined and evaluated for air in reference 6. Values of u_l typical of the two run conditions used for p_1 were 8595 m/sec and 6550 m/sec and are shown in table 1. Variations in u_l are expected as a result of variations in bursting pressure in the driver chamber and ambient temperature. The standard deviation from the mean value of u_l for 30 runs was ±3 percent.

The flow-core density ρ/ρ_0 shown in figures 15, 16, 17, and 20 was estimated from the measured velocity and the central pitot pressure. Pitot pressure was measured for several separate runs.

Reproducibility of repeated runs.- A comparison of the velocity and the velocity profile of the expansion-tube flow for repeated runs is shown in figure 15. The average values of the results of eight expansion-tube runs are plotted. The deviation indicated at each data point is the standard deviation from the mean at that position of the tube radius. These results show that the flow-core velocities were reproducible to about ±2.5 percent. The velocity profiles were reproducible to about ±0.7 percent in the flow core and about

±6 percent in the boundary flow. Figure 15 also indicates that there is a flow core with a radius of approximately 45 percent of the tube radius in which the flow velocity is uniform to within ±0.7 percent.

Velocity profile.- In figure 16 the velocity profiles about 50 μsec behind the interface are plotted for different values of p_{10}. The results show a core of uniform flow velocity with a radius of about 40 percent of the tube radius and a slight increase in core radius with an increase in p_{10} and corresponding increase in ρ/ρ_0. For each condition in figure 16(a), the core radius for which the velocity is uniform within 5 percent ranges from 50 to 60 percent of the tube radius.

In each part of figure 17 the velocity-profile results are plotted for a given value of p_{10} and for various times behind the He-air interface. This figure shows a flow core of uniform velocity for each condition over the range of times Δt_1 measured. There is an indication that the shape of the velocity profile is beginning to change at the later values of Δt_1 in each part of the figure.

Boundary layer.- A boundary-layer thickness $\delta_{0.95}$, where the velocity of the flow has fallen off to 95 percent of the core velocity, was estimated for each run. The averages of these results are shown in figure 18. For times later than 50 μsec the results indicate a slight decrease in the boundary-layer thickness with an increase in Δt_1 and with an increase in p_{10}. The boundary-layer thickness $\delta_{0.99}$ for the He flow just ahead of the He-air interface, which was estimated by using reference 7, is shown in figure 18(a). The maximum values of the boundary-layer thickness obtained for the air flow are about two times the estimated boundary-layer thickness in the He flow ahead of the interface.

A laminar boundary layer was indicated for all the run conditions by the data from thin-film gages and pressure transducers.

Velocity.- The normalized core velocity u_c/u_l as a function of the time behind the He-air interface and p_{10} is shown in figure 19. The variation of the core velocity over a range of 150 μsec is about 8 percent. The core velocities u_c for figure 19(a) lie between 5900 m/sec and 6700 m/sec. All the velocities which are presented in figure 19(a) can be included within a velocity spread of about 11 percent.

Figure 19(b) shows an increase in velocity with a decrease in p_{10} for the two conditions of p_1 used. Figure 19(b) also shows the velocity that would be predicted by theory as p_{10} is varied. The prediction was made by equating the helium shock velocity to the interface velocity (the asymptote of the leaky piston theory (ref. 7)) and by equating the pressure behind the helium shock to the pressure of the air expanded in equilibrium. The pressure rise in the helium between shock and interface was thus neglected. The runs at $p_1 = 100$ torr $= 13\ 300$ N/m^2 fall somewhat above the predictions, while the runs

at $p_1 = 22$ torr $= 2930$ N/m^2 were less than predicted. At low values of p_{10} the measured velocity does not approach u_l as rapidly as predicted, a result which may be due to viscous losses in the expansion.

Density.- Figure 20 shows the variation of the flow-core density ρ/ρ_0 with Δt_1 and p_{10}. The density was computed from the relation $\rho = p_t/u_c^2$, where ρ is the density, p_t is the central pitot pressure, and u_c is the core velocity.

Figure 20(a) shows a continual increase in density with time for the lowest value of p_{10} and a decrease followed by an increase for the highest value of p_{10}. It should be noted that for the lowest value of p_{10} used, the expansion fan arrives early in the flow and the velocity measurements were all made after the arrival of the expansion fan. Variations in the density by factors of 1.5 to 5 are indicated by the data for a time interval of about 150 μsec behind the He-air interface as compared with factors of only 1.1 to 1.3 for data obtained in the time interval between the He-air interface and the arrival of the expansion fan, which is defined as the expansion-tube test time.

Figure 20(b) shows a decrease in the density with decreasing p_{10}. A comparison of figures 19 and 20 shows that the core density is a much more rapidly varying function of Δt_1 and p_{10} than the core velocity.

CONCLUSIONS

A method of measuring the velocity profile of the free-stream flow in the Langley pilot model expansion tube was developed and tested. Conclusions 1 to 5 were reached with regard to the method of measuring the velocity; conclusions 6 to 10 concern the properties of the flow and were obtained from results of the velocity measurements over a range of flow-core density ρ/ρ_0 (where ρ is the gas density and ρ_0 is the gas density at standard conditions) from 3×10^{-4} to 2×10^{-3} and times behind the He-air interface of up to about 150 μsec. These conclusions are as follows:

1. The flowing gas was tagged or identified by partial ionization with the use of ultraviolet light.

2. The position of the ionized region could be detected or located by passing a current through the ionized region.

3. Only a qualitative agreement was observed between the shape of the ionized region and the detected region, with the agreement appearing to be better for flow conditions than for static conditions.

4. A luminous region not directly associated with the flow appears near the source electrode. This effect does not allow the displaced ionized region to be observed near this electrode.

16

5. Velocity profile data could be obtained for velocities of the order of 6300 m/sec and over a range of flow-core density ρ/ρ_0 from 3×10^{-4} to 2×10^{-3}.

6. There is a flow core with a radius in the range of 50 to 60 percent of the tube radius in which the velocities lie within a range of 5 percent. Within a flow-core radius up to 45 percent of the tube radius, velocities were observed that were uniform to about ±1 percent.

7. There is a slight decrease in the boundary-layer thickness with an increase in the core density and with increasing time behind the He-air interface.

8. The velocities measured for a repeated-run condition were reproducible to within ±2.5 percent.

9. The variation of the core velocity lies within a range of 8 percent over a range of 150 μsec behind the He-air interface.

10. The flow-core densities estimated from measured velocities and pitot pressures indicate variations of factors of about 1.5 to 5 over the range of about 150 μsec behind the He-air interface. However, within the expansion-tube test time, which is the interval between the He-air interface and the arrival of the expansion fan, variations in the core density of factors of only 1.1 to 1.3 were indicated by the data.

Langley Research Center,
    National Aeronautics and Space Administration,
        Langley Station, Hampton, Va., September 9, 1968,
            129-01-02-02-23.

REFERENCES

1. Jones, Jim J.; and Moore, John A.: Exploratory Study of Performance of the Langley Pilot Model Expansion Tube With a Hydrogen Driver. NASA TN D-3421, 1966.

2. Kyser, James B.: Development of a Tracer-Spark Technique for the Study of Hypervelocity Flow Fields. Third Hypervelocity Techniques Symposium, Univ. of Denver and Arnold Eng. Develop. Center, Mar. 1964, pp. 336-363.

3. Fletcher, R. C.: Production and Measurement of Ultra-High Speed Impulses. Rev. Sci. Instrum., vol. 20, no. 12, Dec. 1949, pp. 861-869.

4. Samson, James A. R.; and Cairns, R. B.: Absorption and Photoionization Cross Sections of O_2 and N_2 at Intense Solar Emission Lines. J. Geophys. Res., vol. 69, no. 21, Nov. 1, 1964, pp. 4583-4590.

5. Cobine, James Dillon: Gaseous Conductors. Dover Pub., Inc., c.1958, pp. 51-53.

6. Grose, William L.; and Trimpi, Robert L.: Charts for the Analysis of Isentropic One-Dimensional Unsteady Expansions in Equilibrium Real Air With Particular Reference to Shock-Initiated Flows. NASA TR R-167, 1963.

7. Mirels, Harold: Test Time in Low-Pressure Shock Tubes. Phys. Fluids, vol. 6, no. 9, Sept. 1963, pp. 1201-1214.

Flow-events detectors

Field stops

Photomultiplier

Window

Heat sensitive gage

uv source and detector electrodes

Flow

Window

Camera
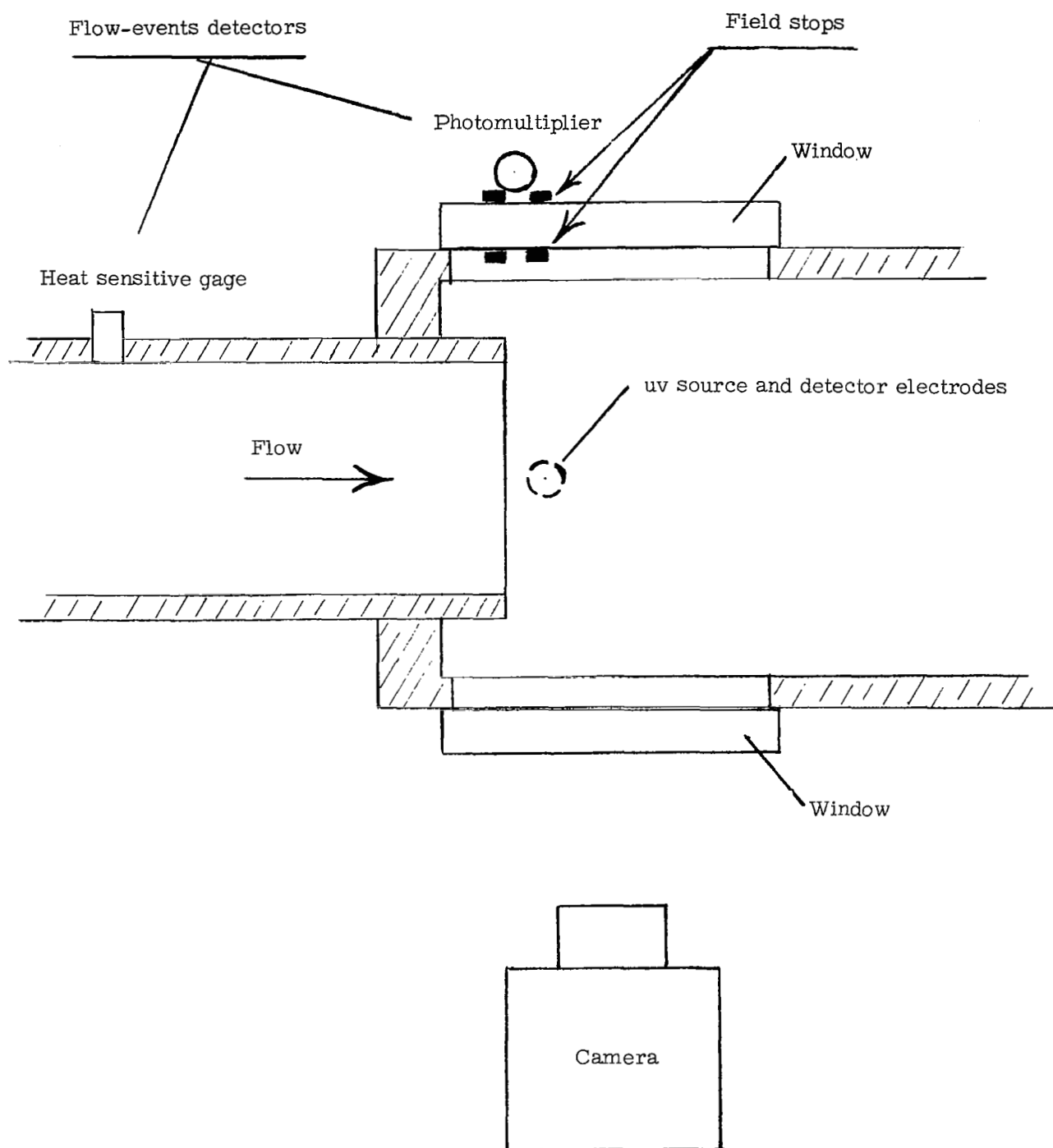
Figure 1.- Arrangement of apparatus at expansion-tube test section. Top view.

uv source

Collimating tube

Flow

$D = .0955 \text{ m}$

0.17 D

1.2 D

Plastic tube

Light pipe to time-interval detector

Detector electrode
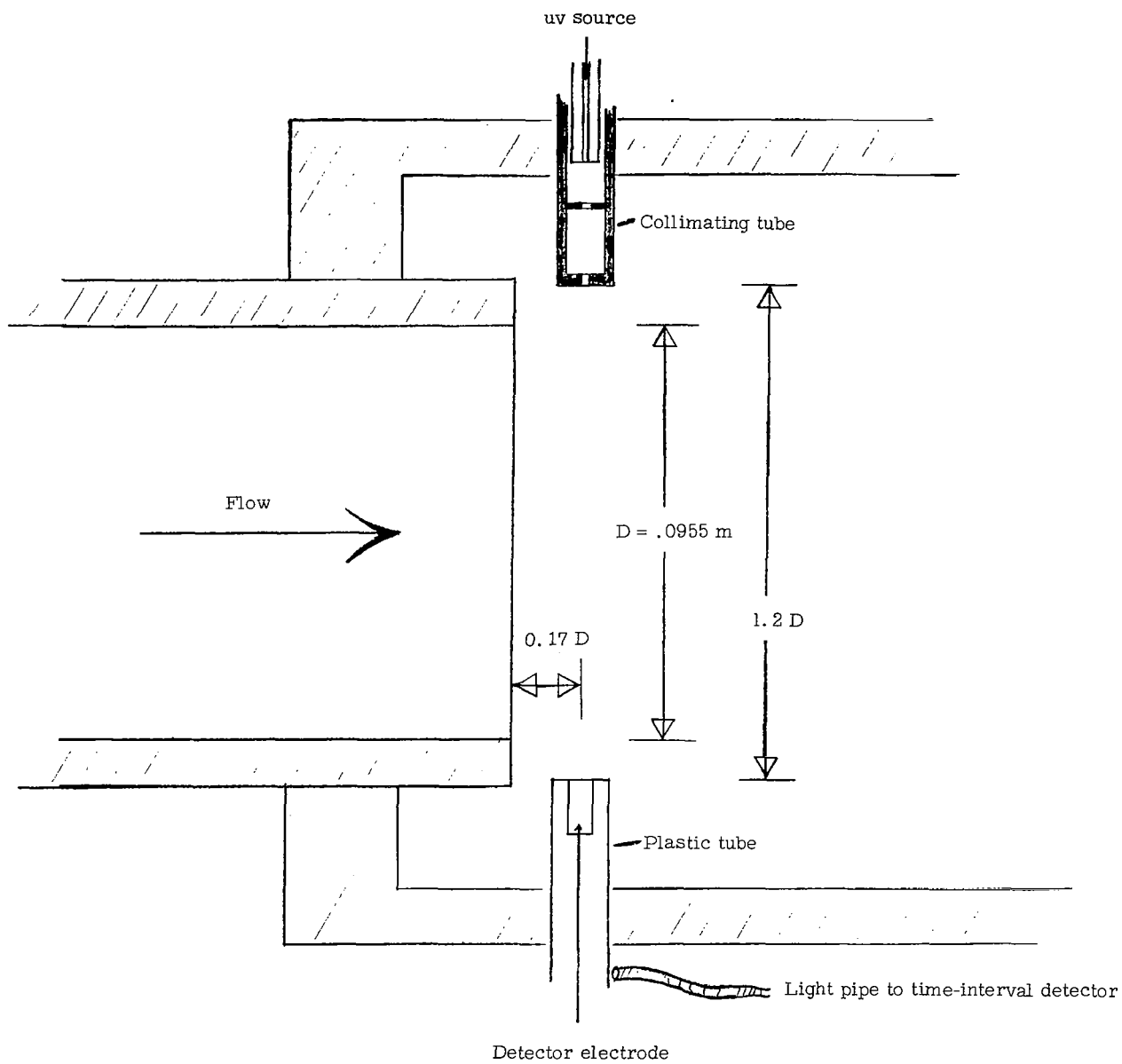
Figure 2.- Position of electrodes in test section.

(-) 40 000 volts

9.1 m

15 MΩ

Coaxial cable RG-8/U

RG-8/U, 1.8 m

Spark-gap
switch

uv source

51 Ω

(a) uv-source pulser circuit.

(+) 20 000 volts

100 MΩ

Coaxial cable

RG-8/U, 9.1 m

Spark-gap switch

RG-8/U, 1.8 m

51 Ω

Detector electrode

26 Ω
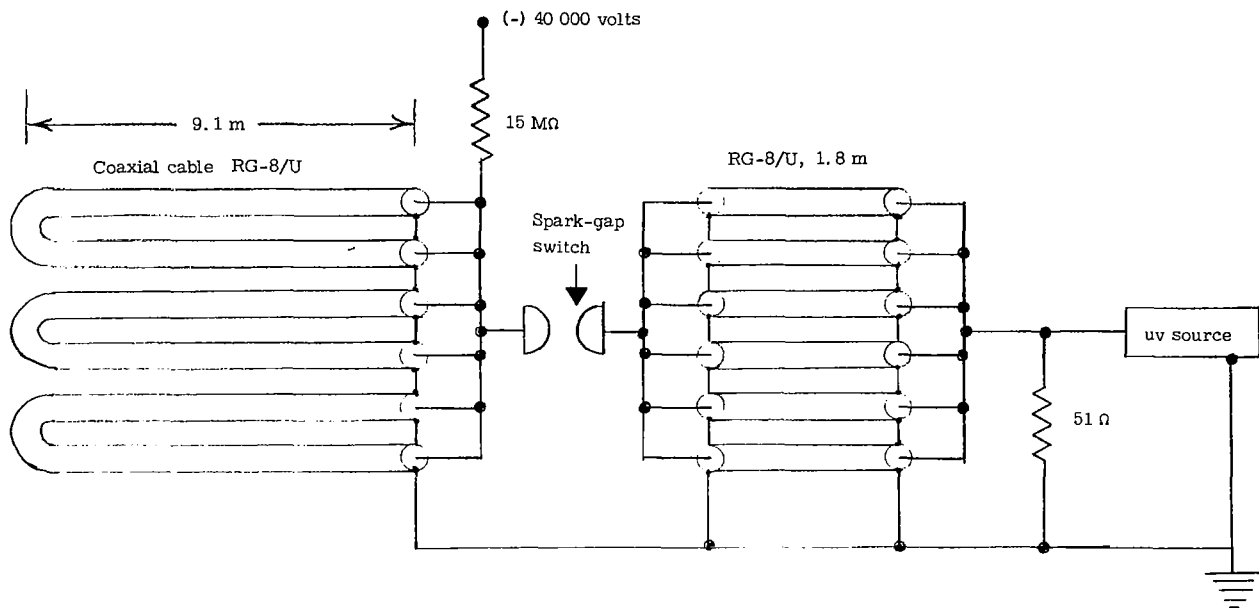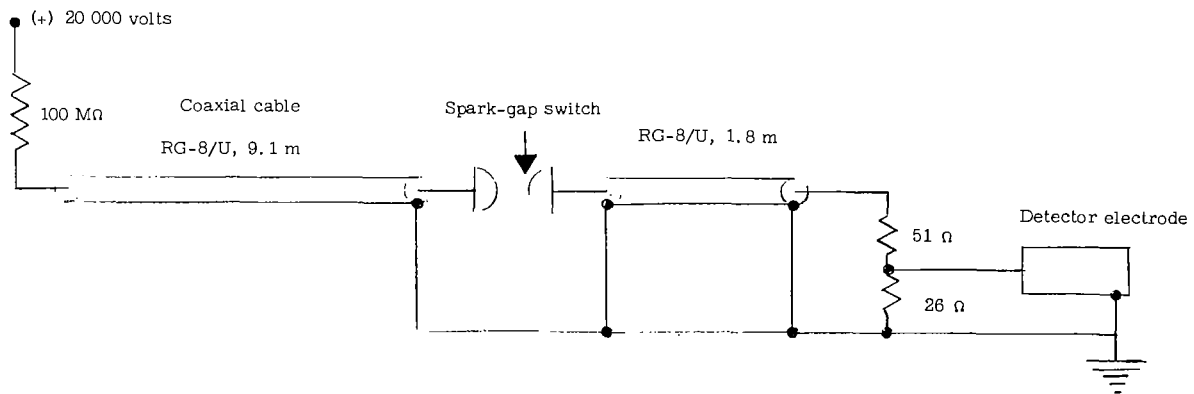
(b) Detector pulser circuit.

Figure 3.- Pulser circuit diagrams.
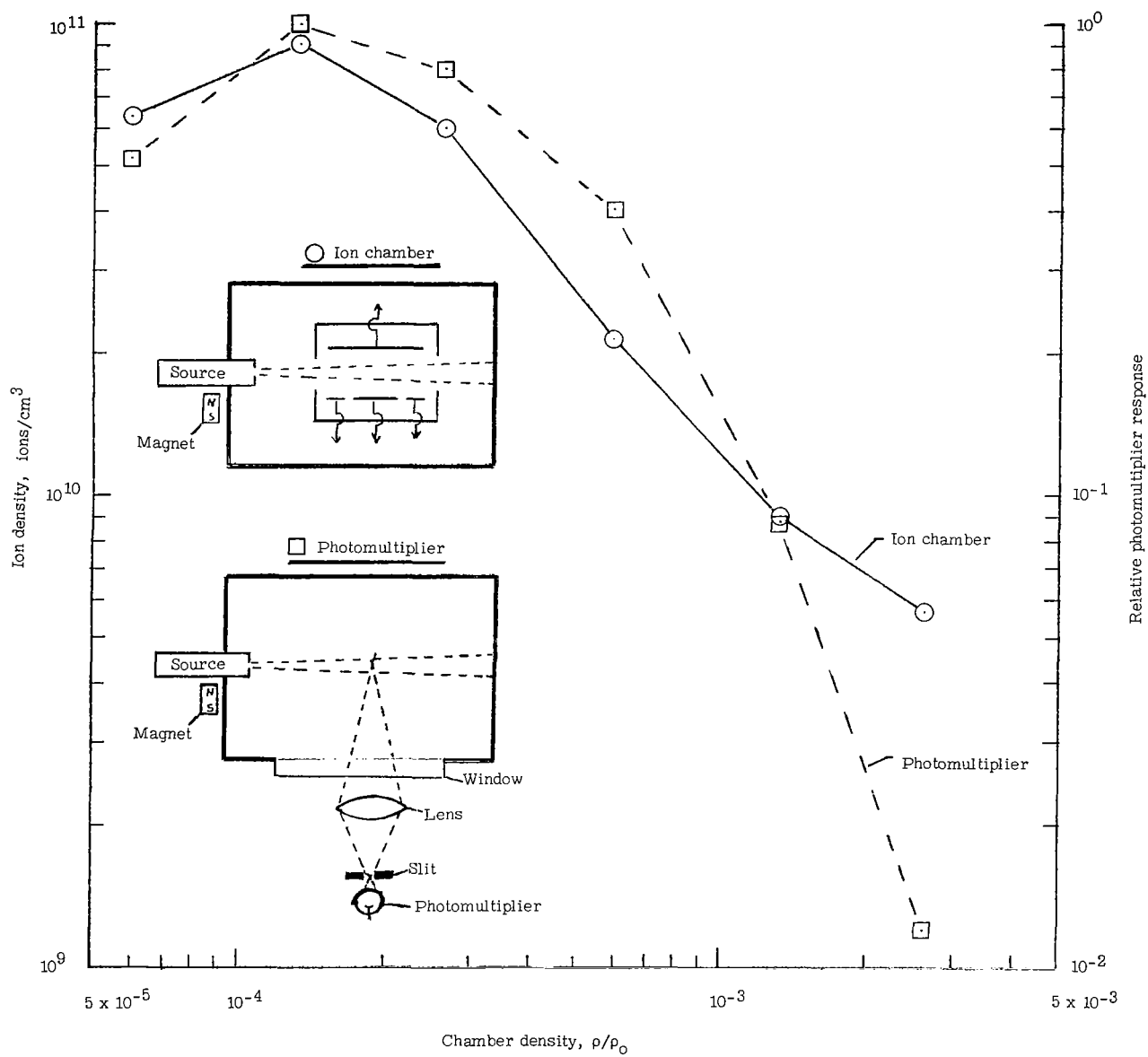
Figure 4.- Variation of ionization and light emission with chamber density at a position 16.5 cm from capillary source. Magnetic field at source.
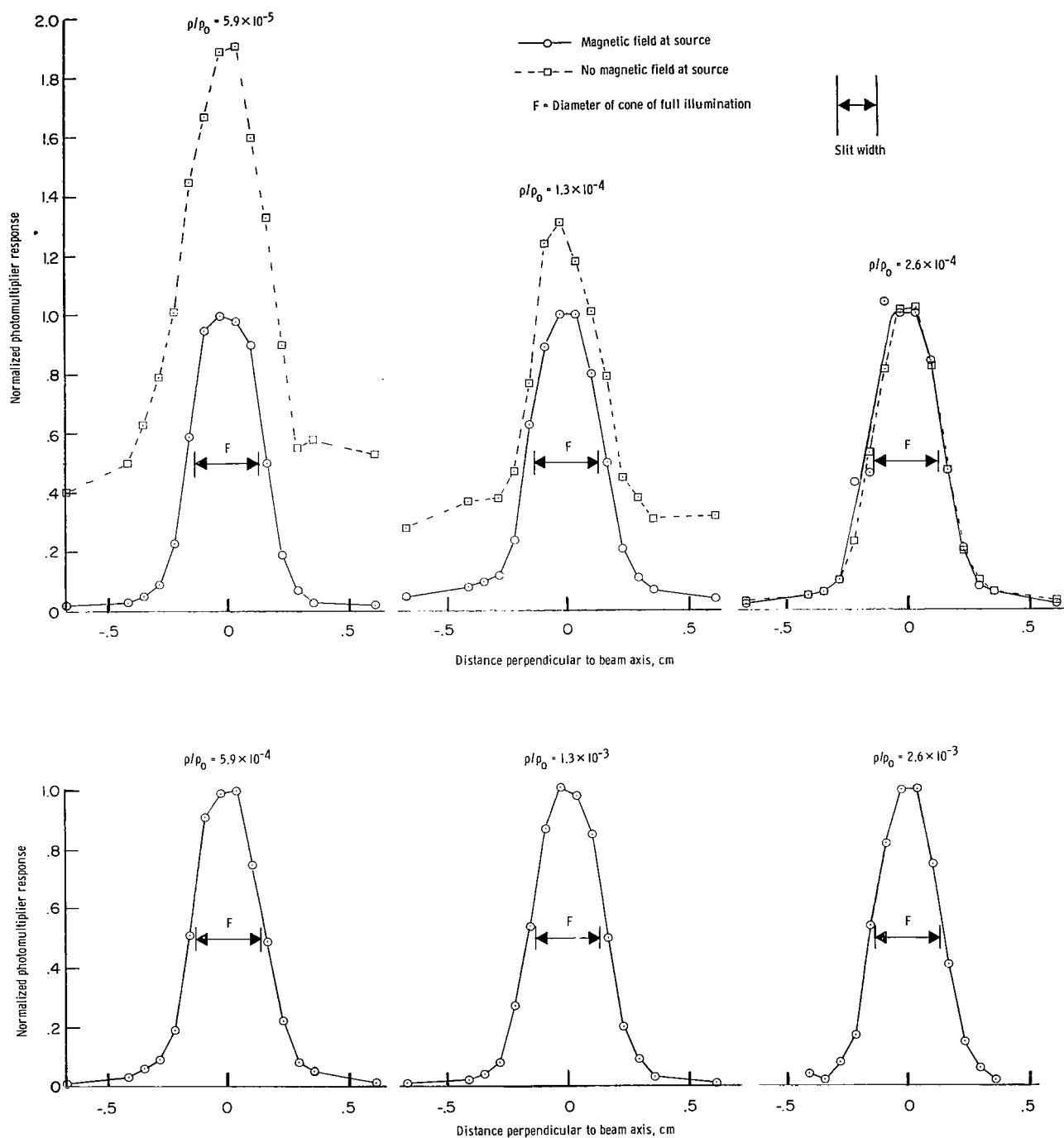
Figure 5.- Comparison of scans, perpendicular to ionizing beam, of light emitted during ionization at a position 13 cm from capillary source.

ρ/ρ_0

O 5.9×10^{-5}
□ 1.3×10^{-4}
◇ 2.6×10^{-4}
△ 5.9×10^{-4}
◺ 1.3×10^{-3}
◿ 2.6×10^{-3}

10^1

10^0

10^{-1}

10^{-2}

10^{-3}

Relative photomultiplier response

6   8   10   12   14   16   18   20

Distance from capillary source, cm
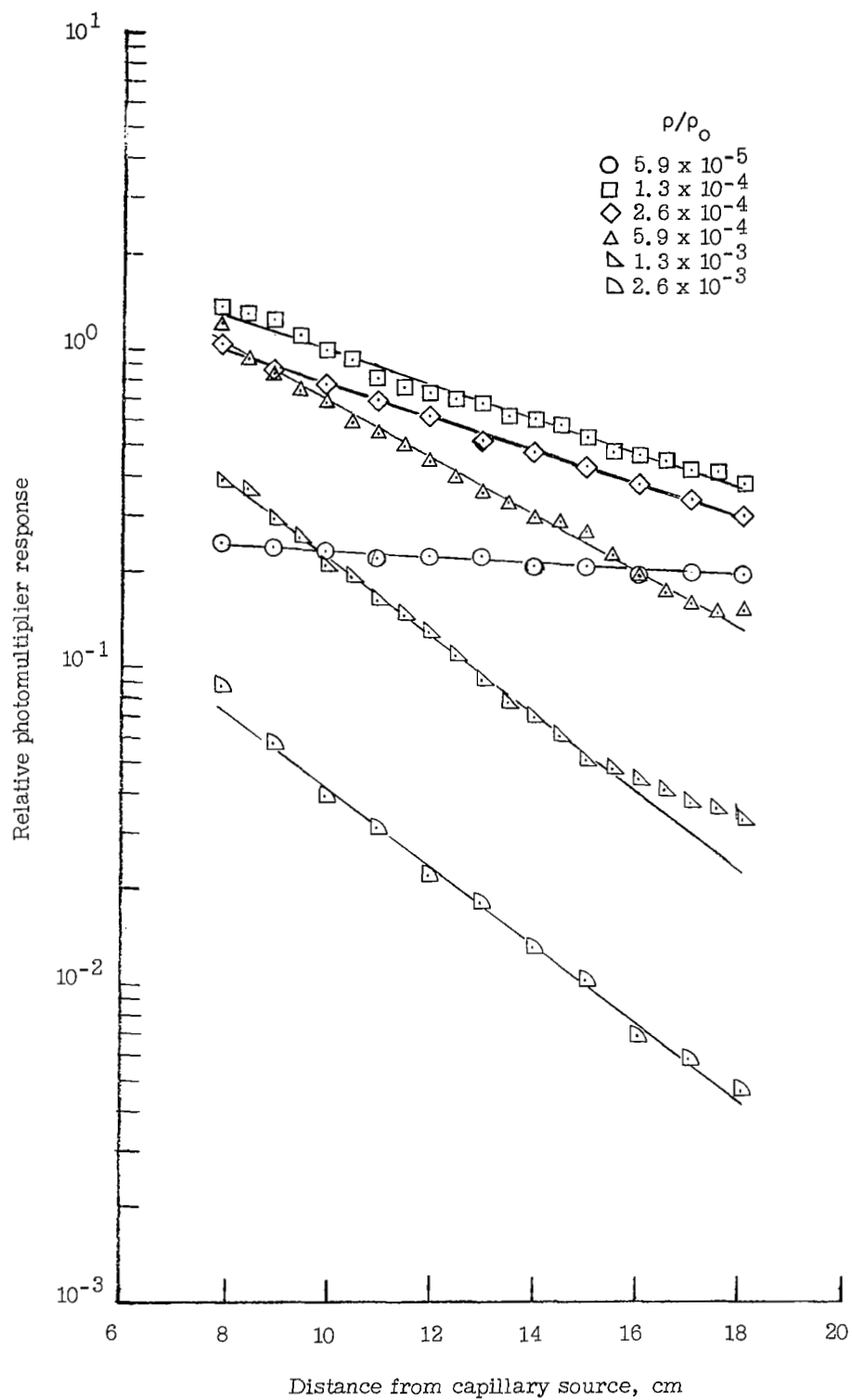
Figure 6.- Variation of light emitted during ionization with position along ionizing beam axis. Magnetic field at source.
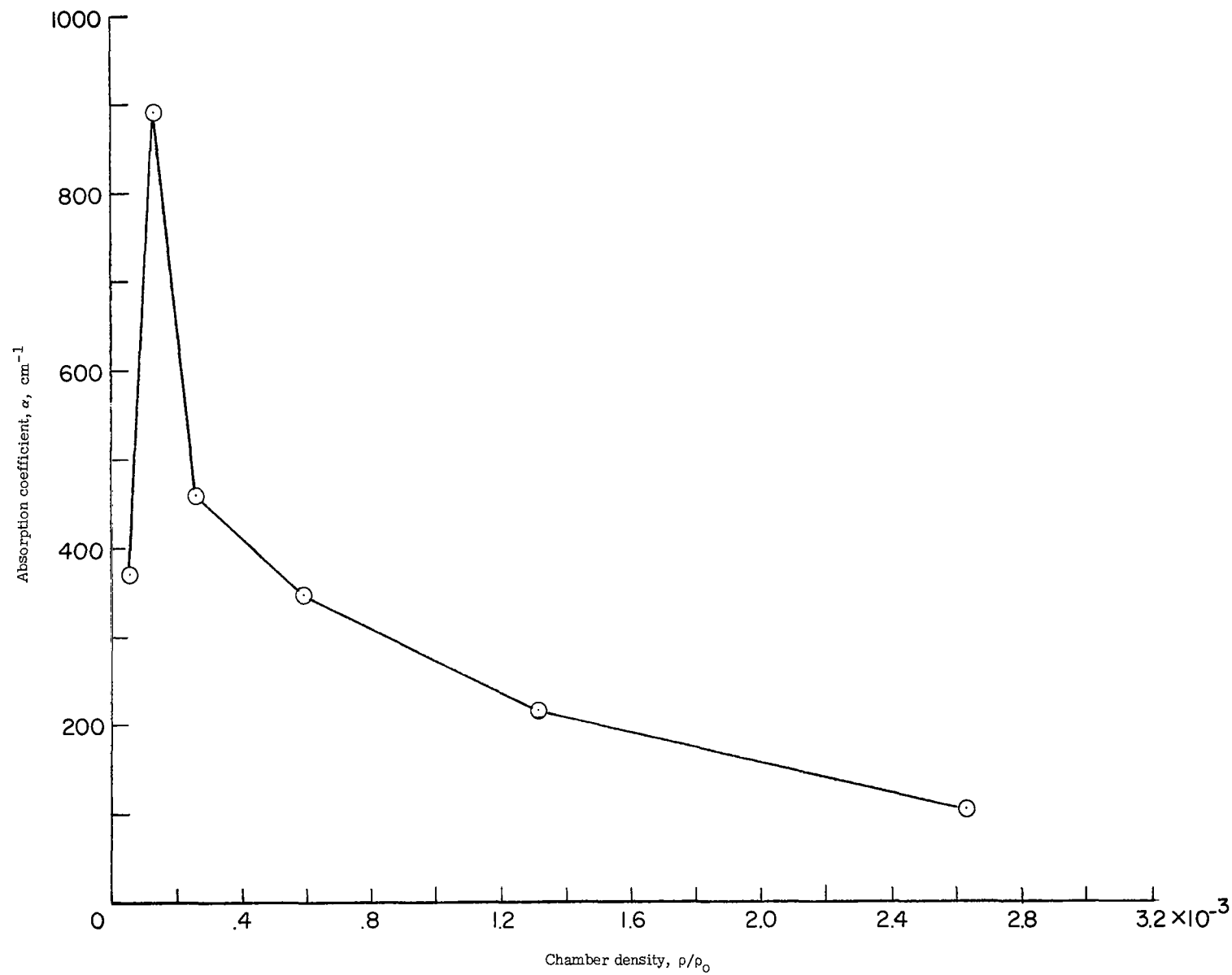
Figure 7.- Variation of effective absorption coefficient with chamber density.
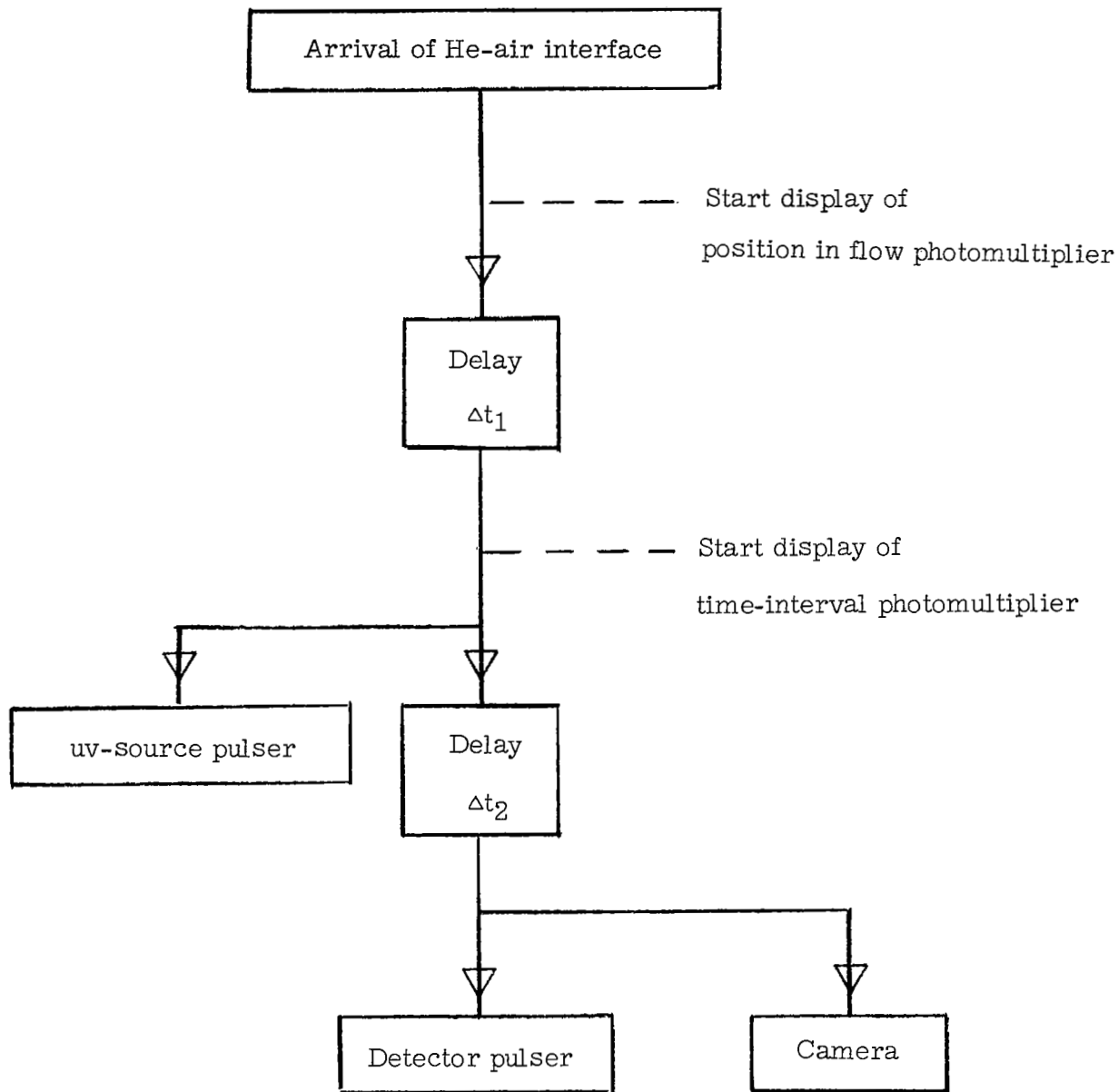
Figure 8.- Sequence of events.
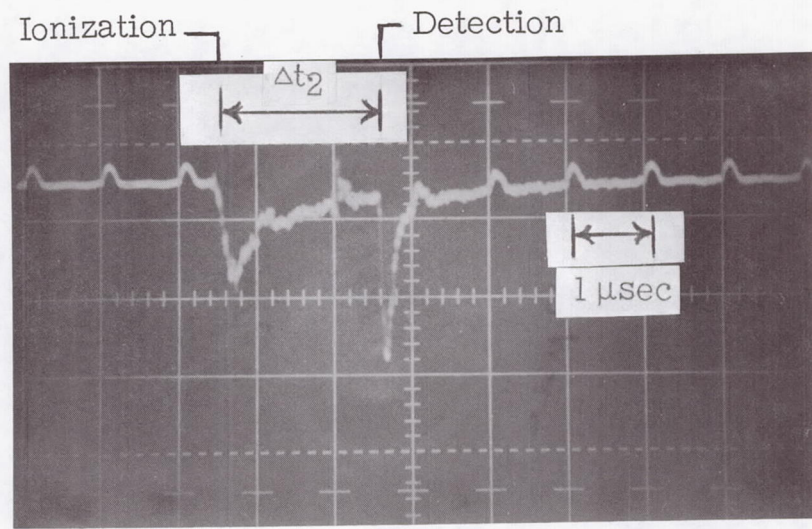
Figure 9.- Sample oscillogram of time-interval photomultiplier trace.
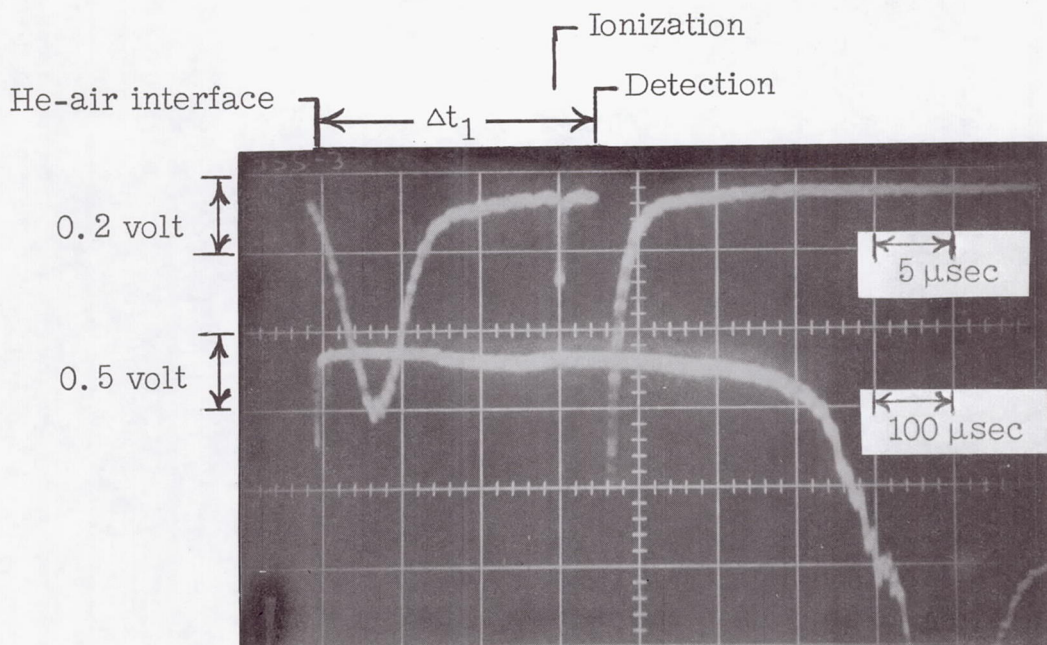
Figure 10.- Sample oscillogram of flow-events detector trace. (Photomultiplier trace shown to two time scales.)
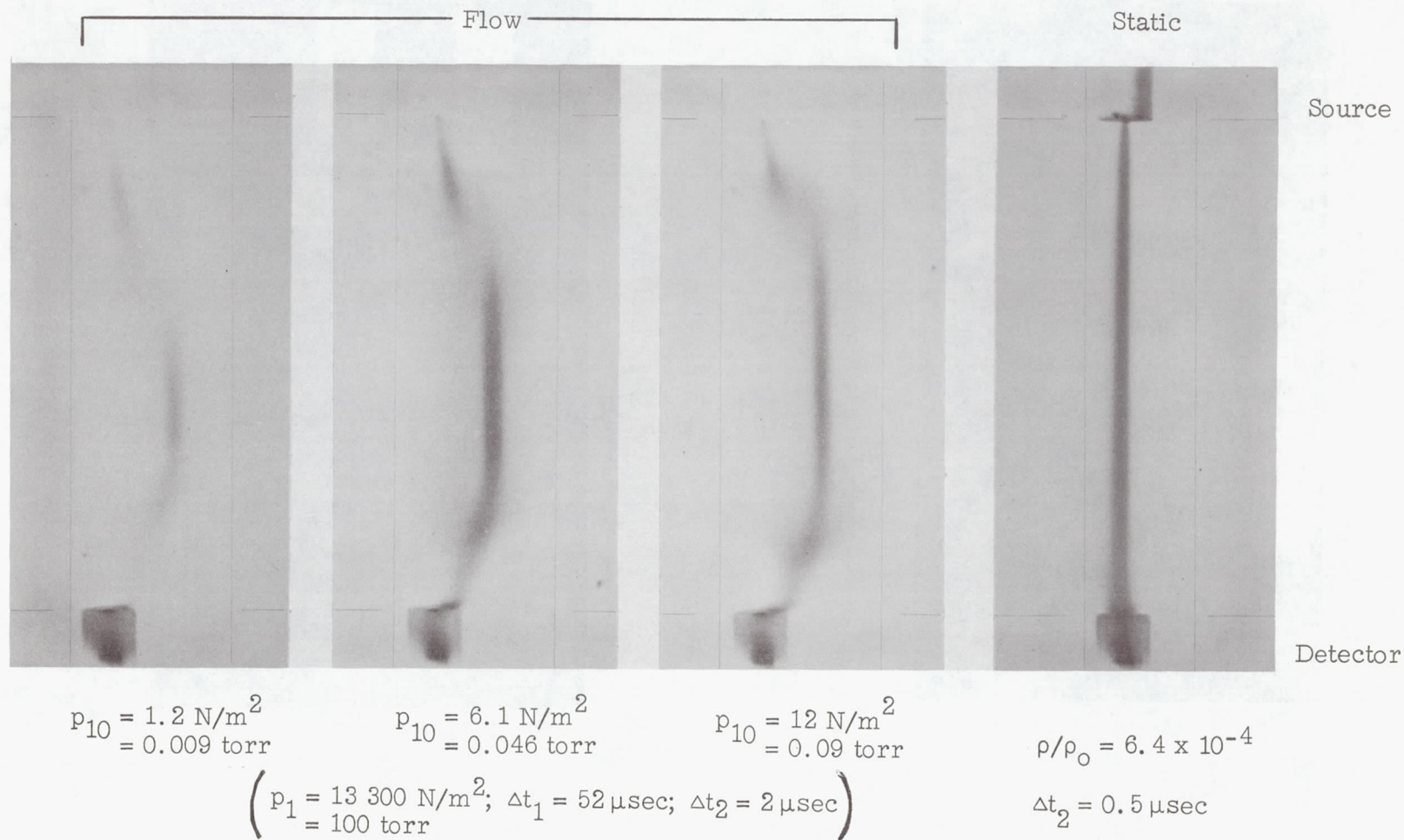
Figure 11.- Photographs of detected ionized region for static and flow conditions.

L-68-8587
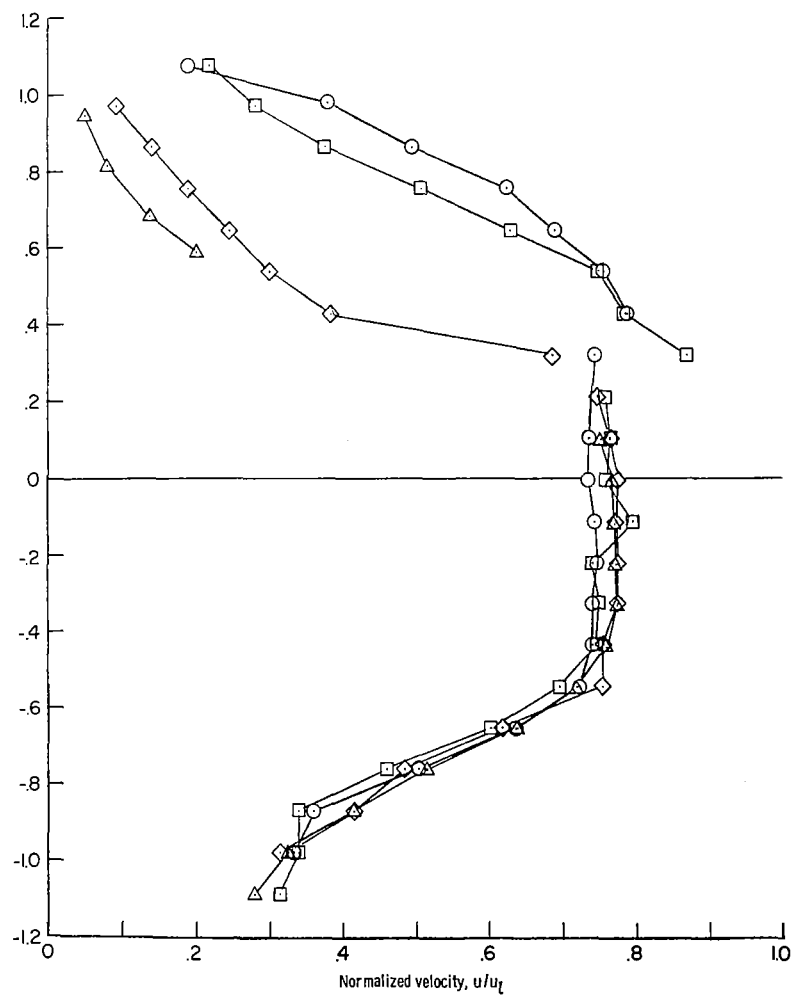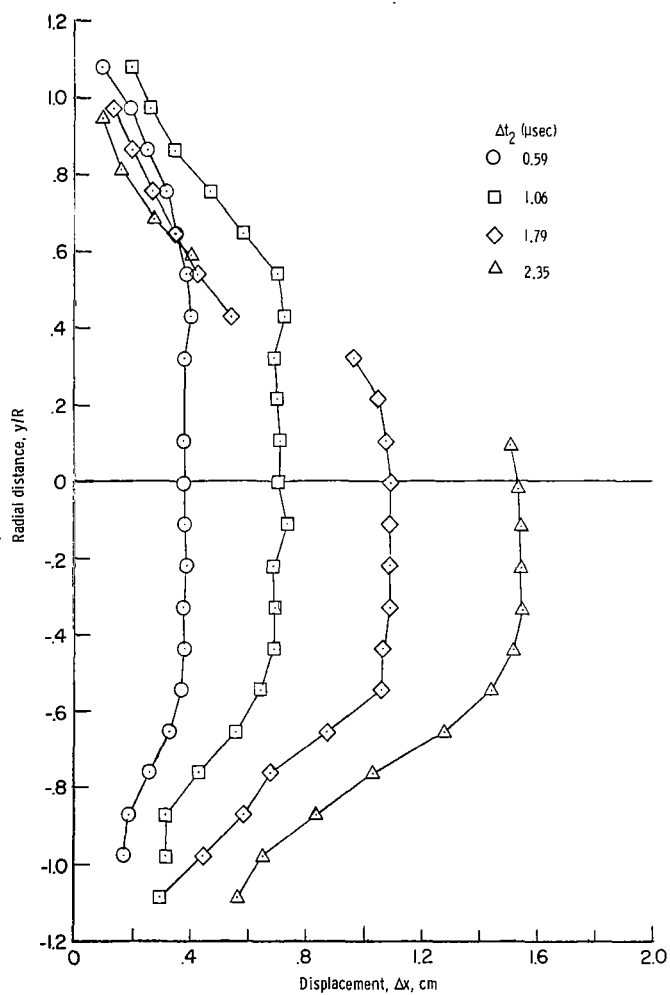
(a) $p_{10} = 0.01$ torr $= 1.3$ N/m^2; $\Delta t_1 = 65$ μsec; $p_1 = 22$ torr $= 2930$ N/m^2.

Figure 12.- Comparison of column displacement with corresponding derived velocity for positions between source and detector electrodes.
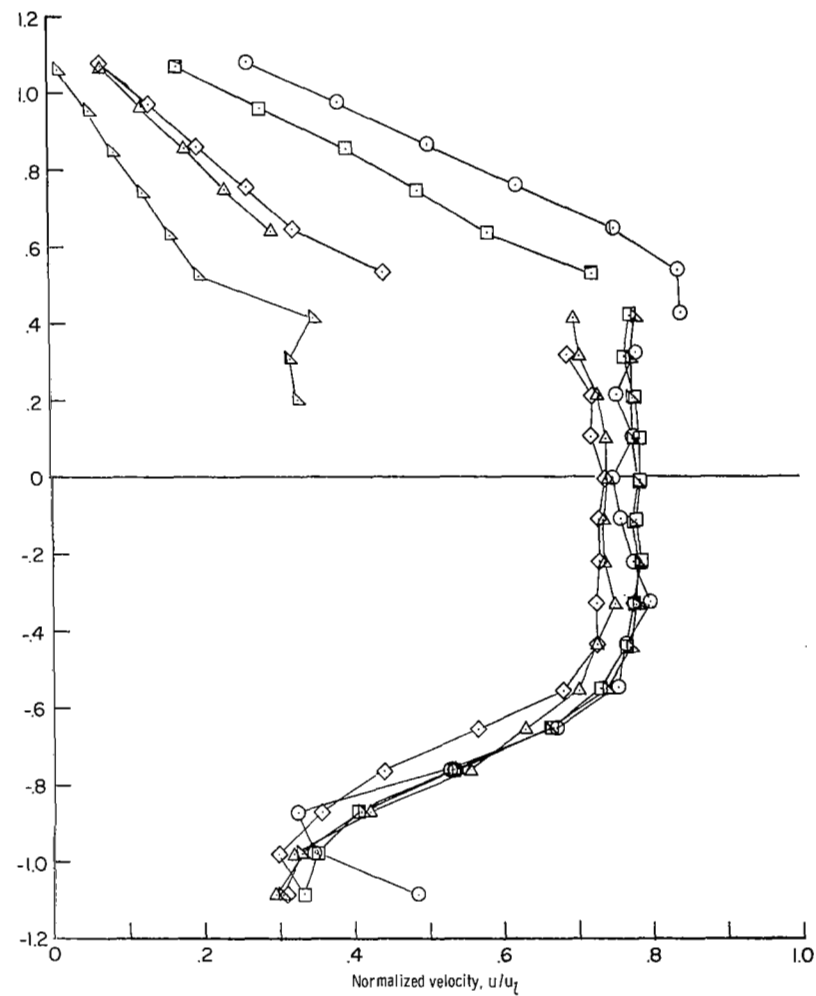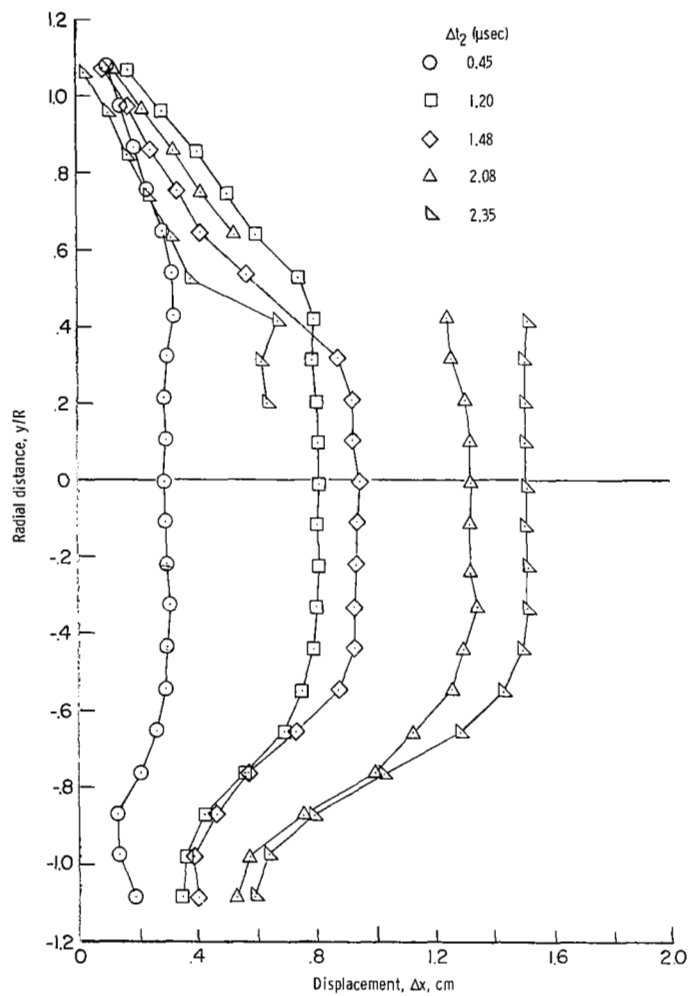
(b) $p_{10} = 0.046$ torr $= 6.1$ N/m2; $\Delta t_1 = 52$ to 64 µsec; $p_1 = 22$ torr $= 2930$ N/m2.

Figure 12.- Concluded.
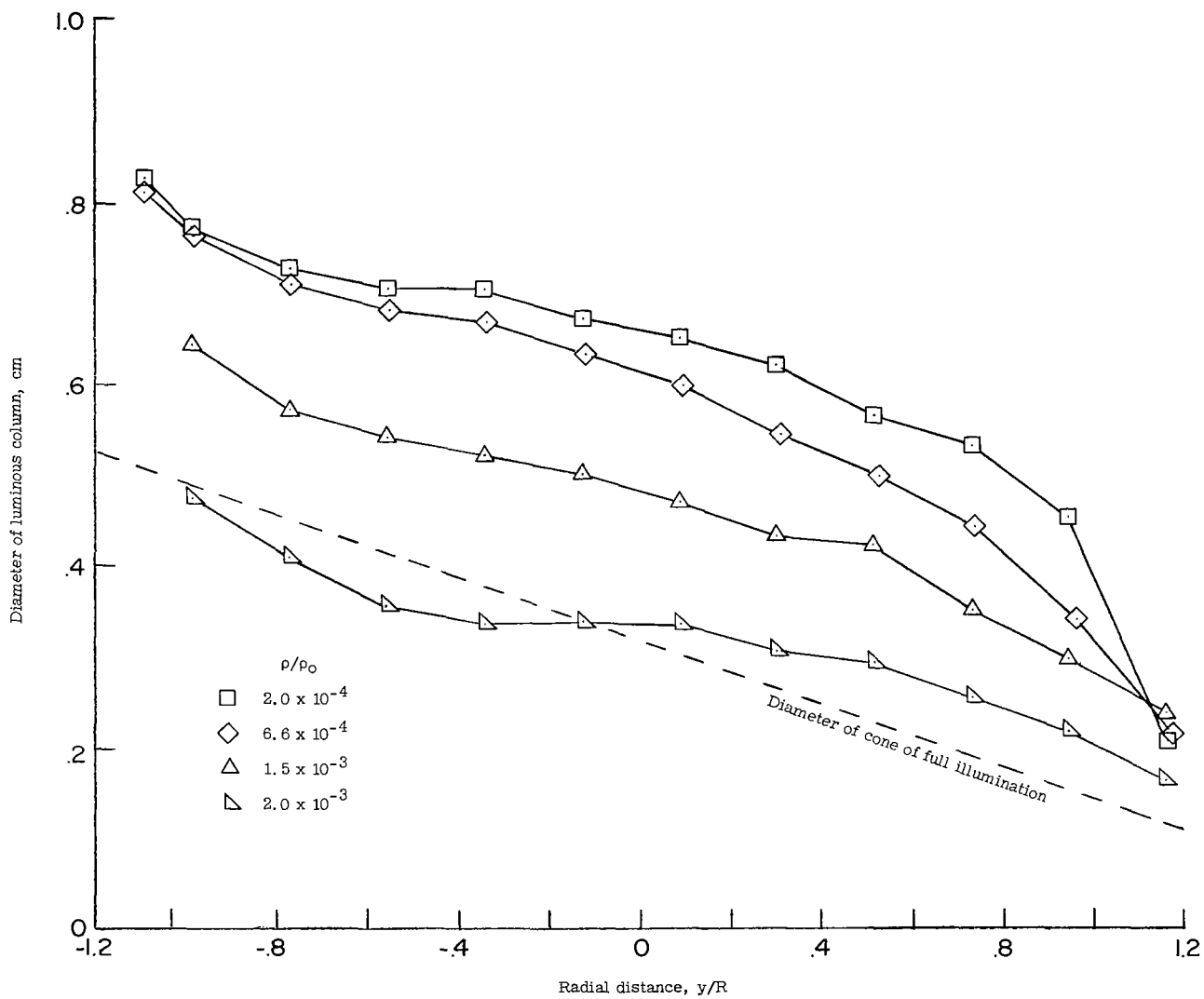
(a) $\Delta t_2 = 0.5$ μsec.

Figure 13.- Variation of diameter of detected luminous column with position for static conditions.
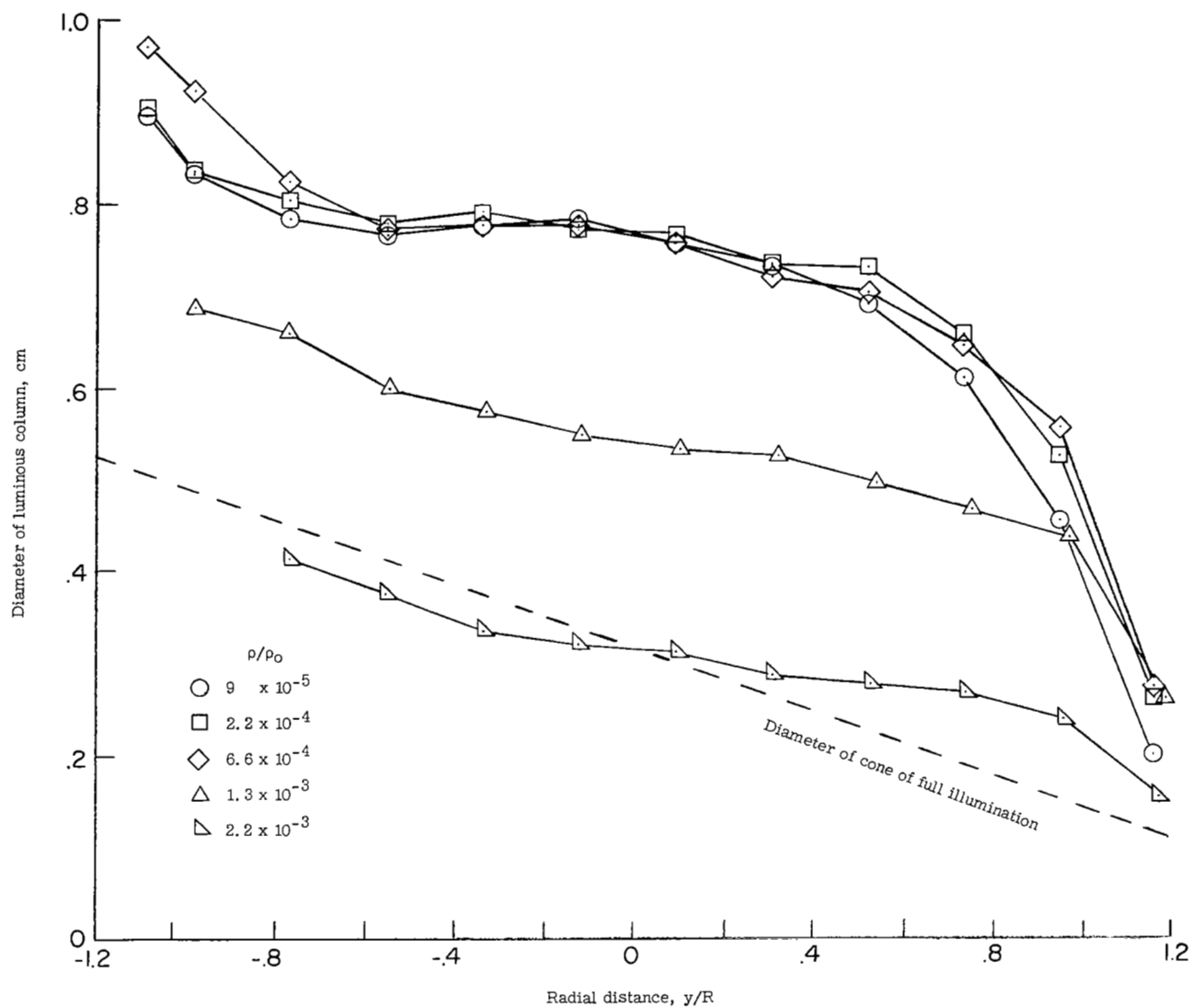
(b) $\Delta t_2 = 2$ μsec.

Figure 13.- Concluded.
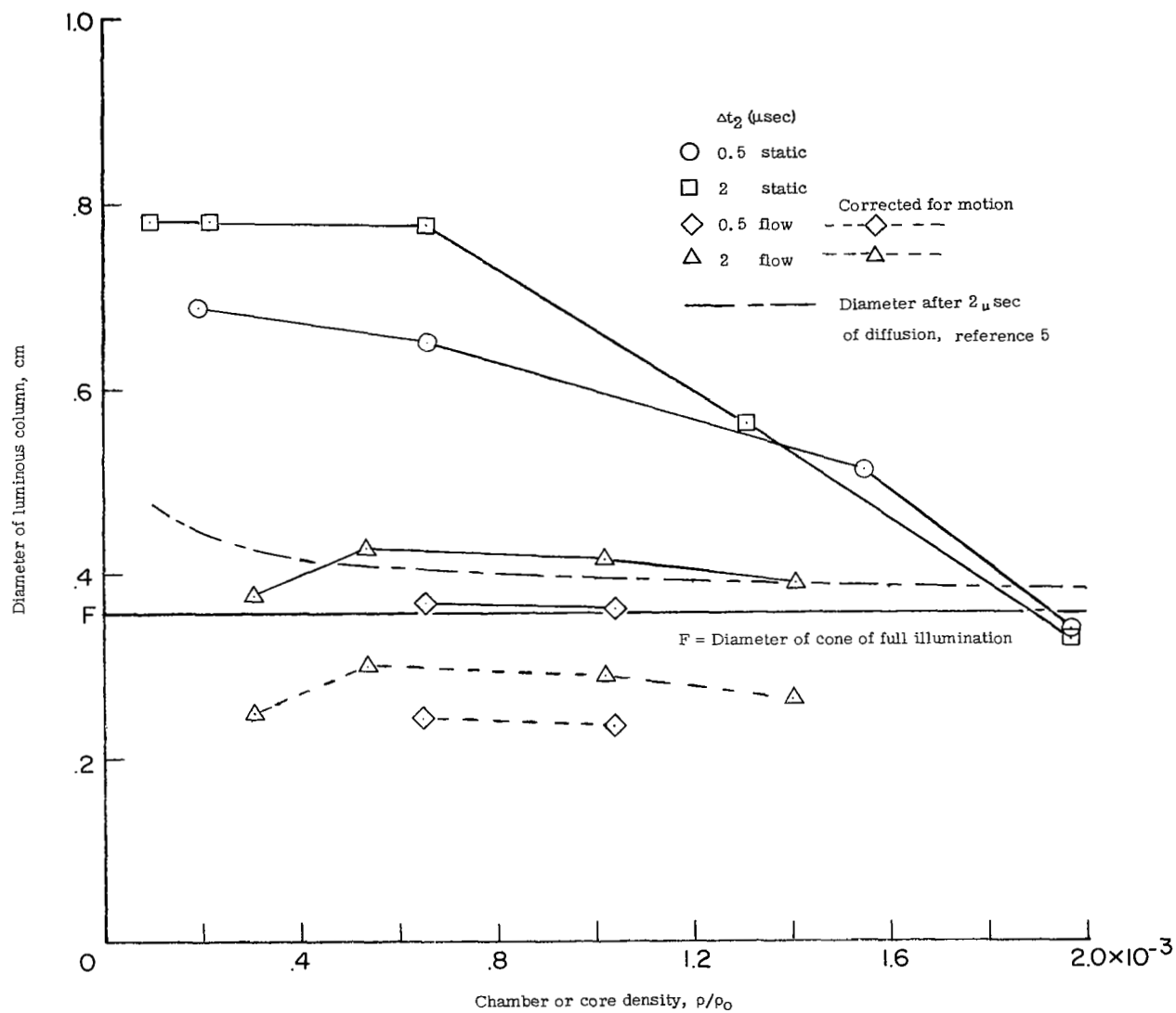
Figure 14.- Variation of diameter of detected luminous column with chamber or core density for static and flow conditions. $y/R = -0.22$.
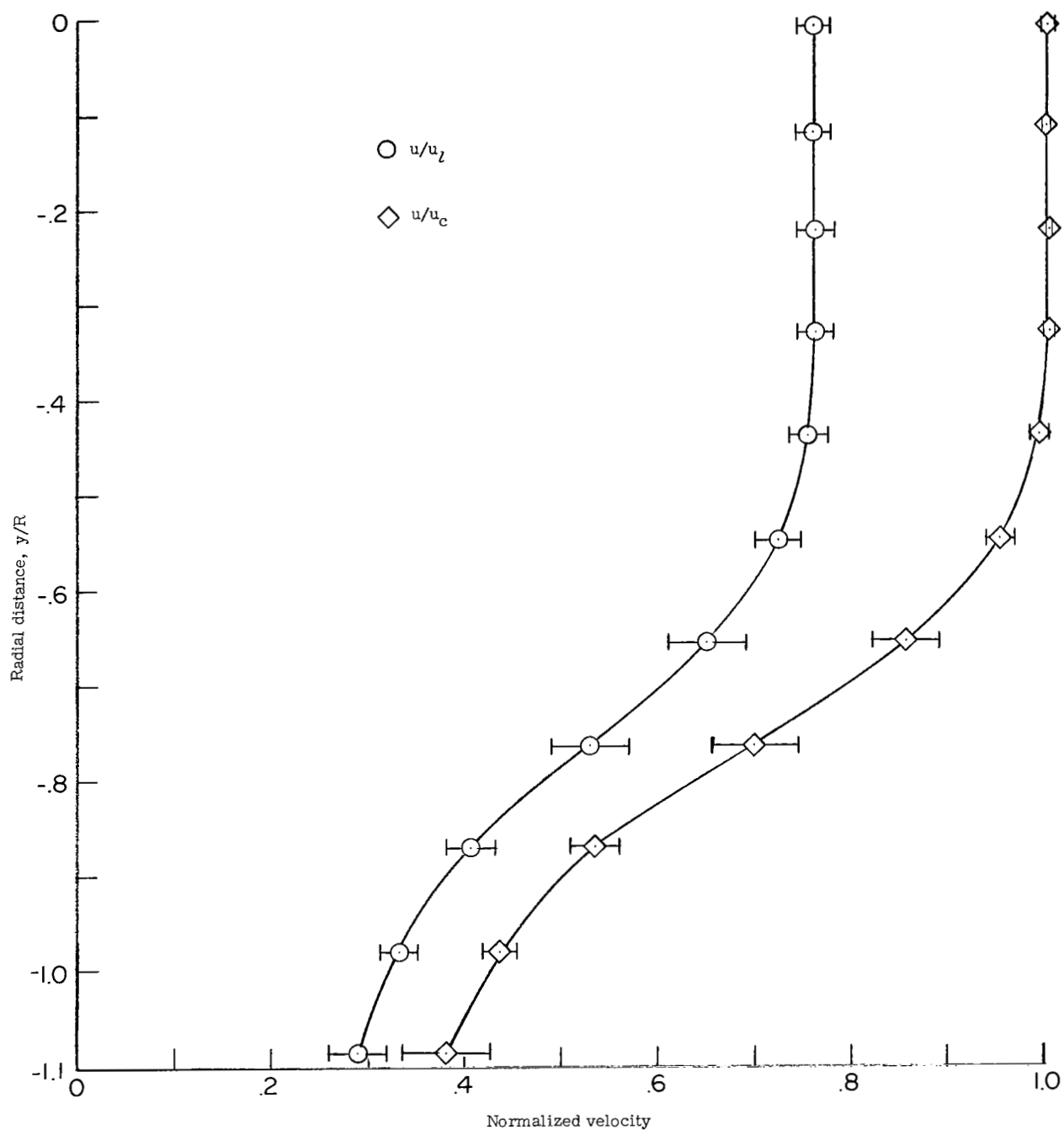
Figure 15.- Comparison of eight repeated expansion-tube runs. $p_1 = 22$ torr $= 2930$ N/m2; $p_{10} = 0.046$ torr $= 6.1$ N/m2; $\Delta t_1 = 54$ μsec; $\rho/\rho_0 = 1.0 \times 10^{-3}$.
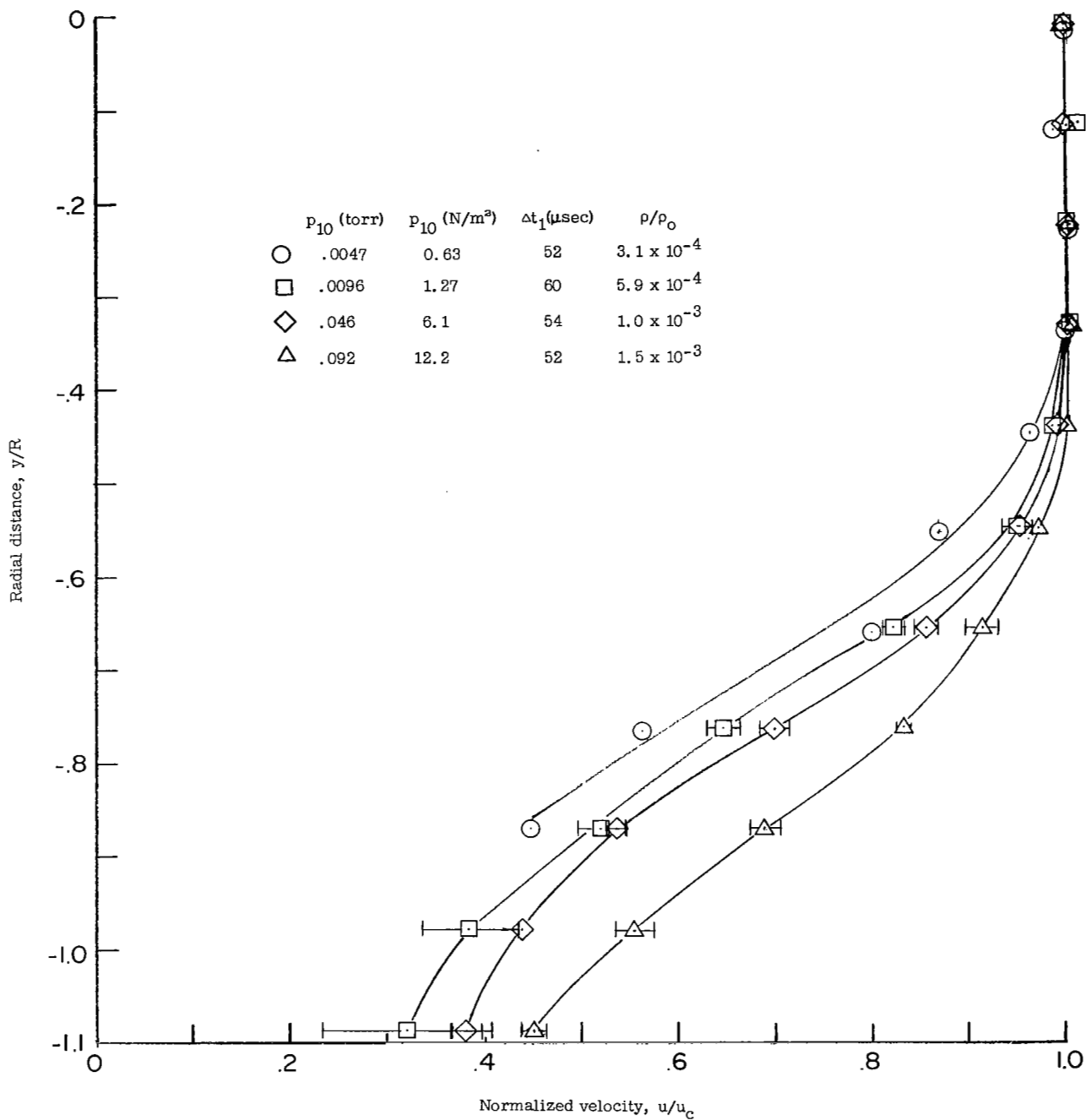
(a) $p_1 = 22$ torr $= 2930$ N/m^2.

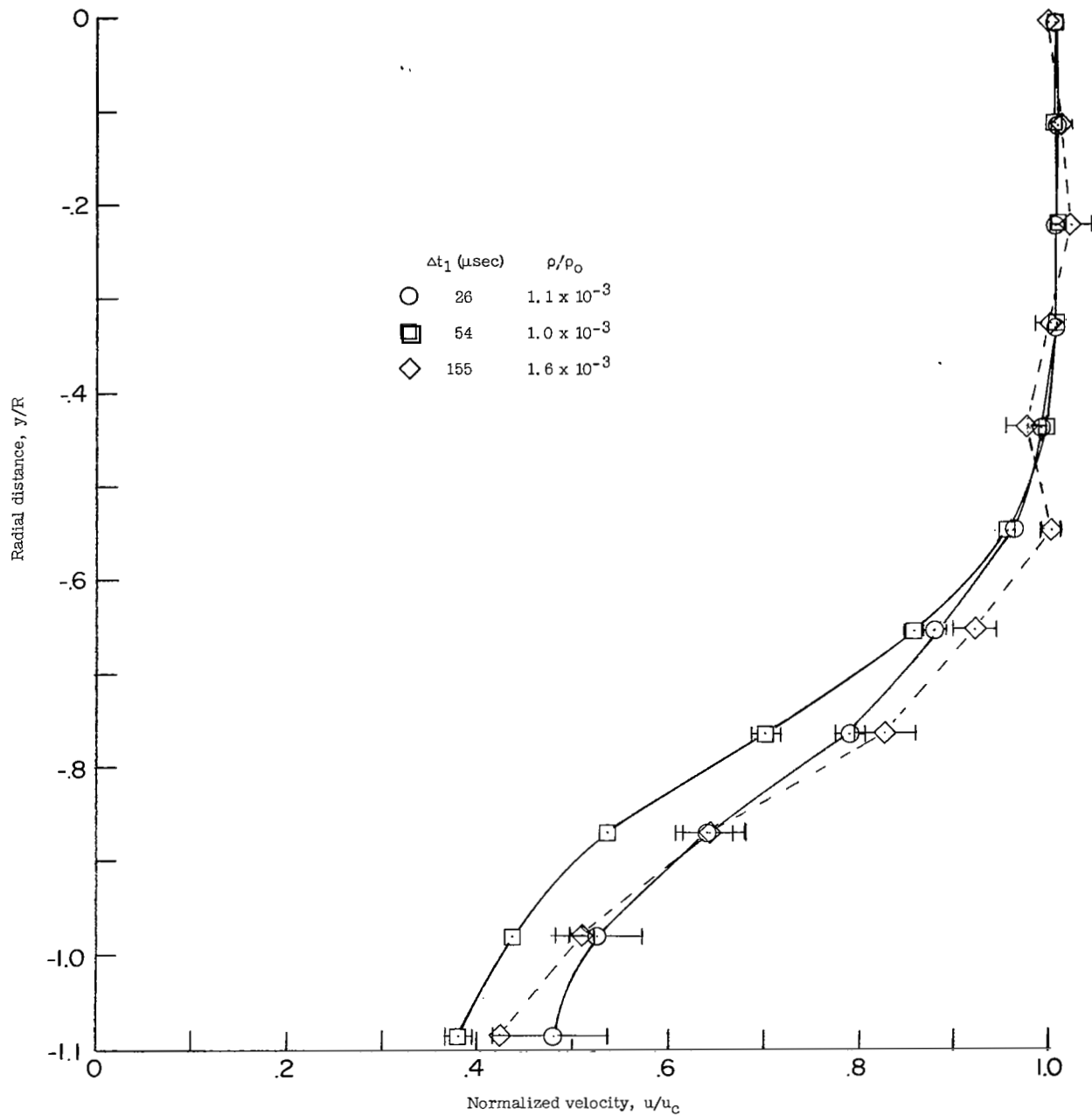Figure 16.- Comparison of velocity profiles for various acceleration chamber pressures.

Figure legend:

p_{10} (torr)	p_{10} (N/m²)
◯ .009	1.2
▢ .046	6.1
◇ .091	12.1
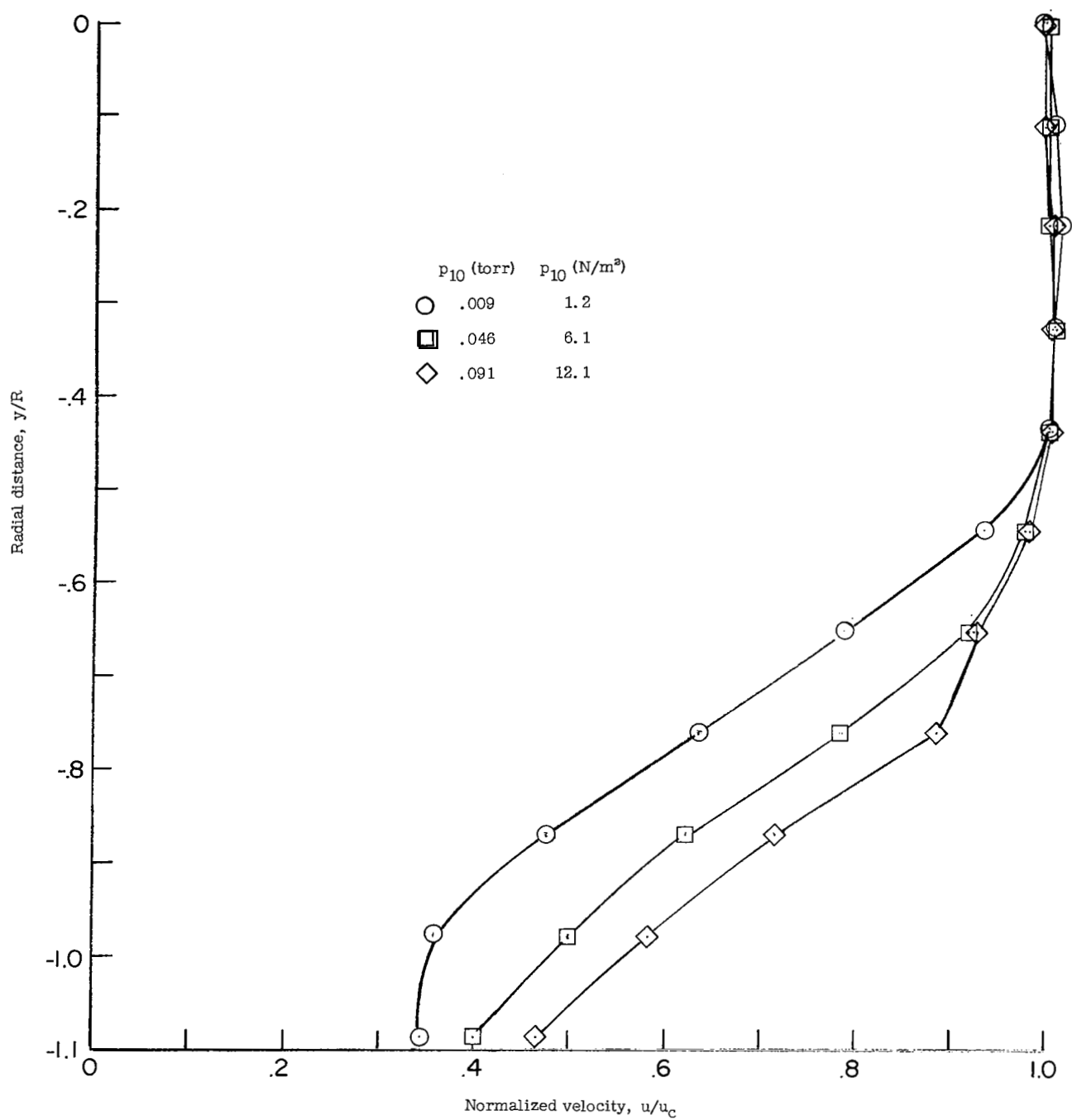
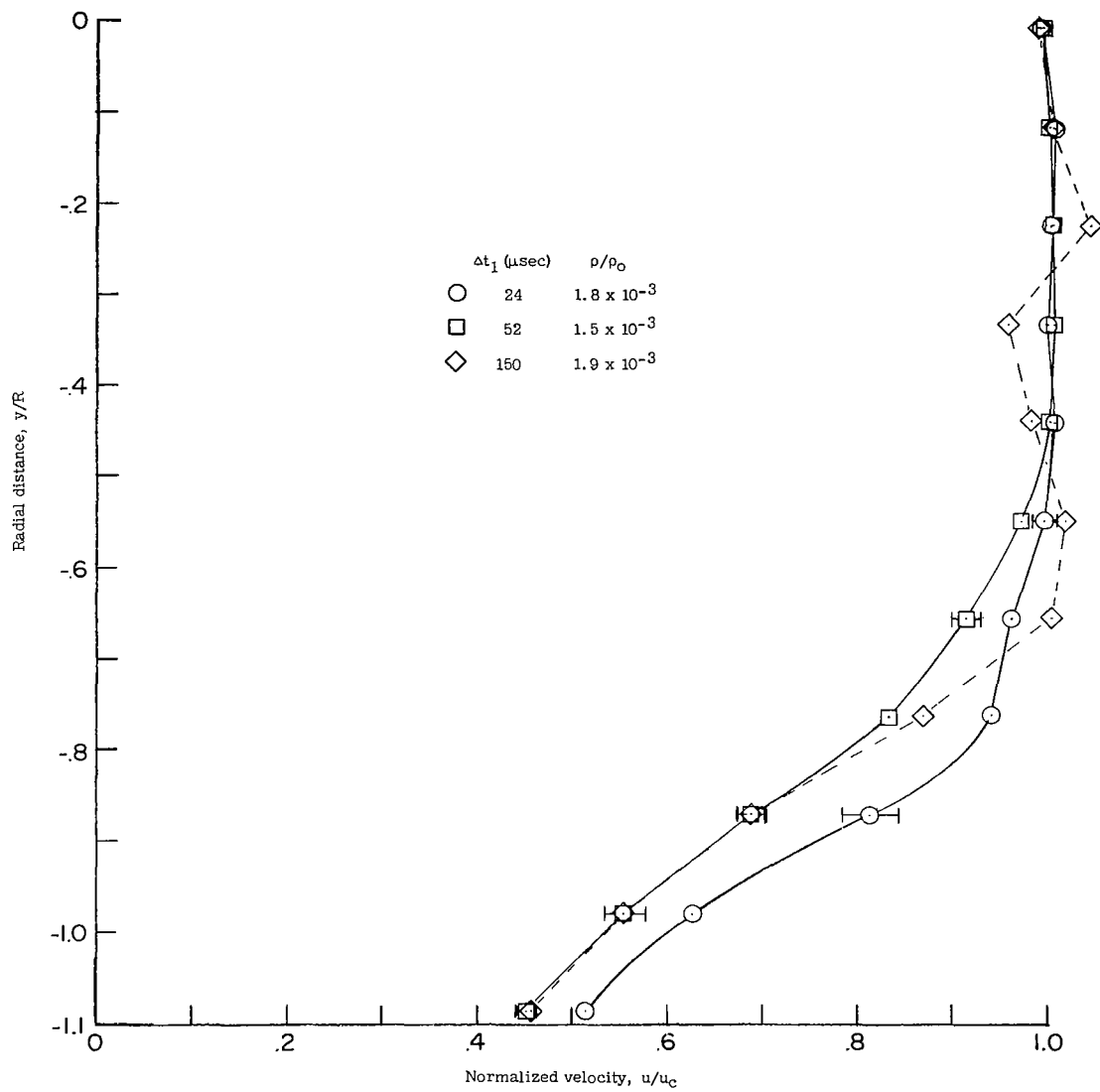(b) $p_1 = 100$ torr = 13 300 N/m²; $\Delta t_1 = 52$ μsec.

Figure 16.- Concluded.
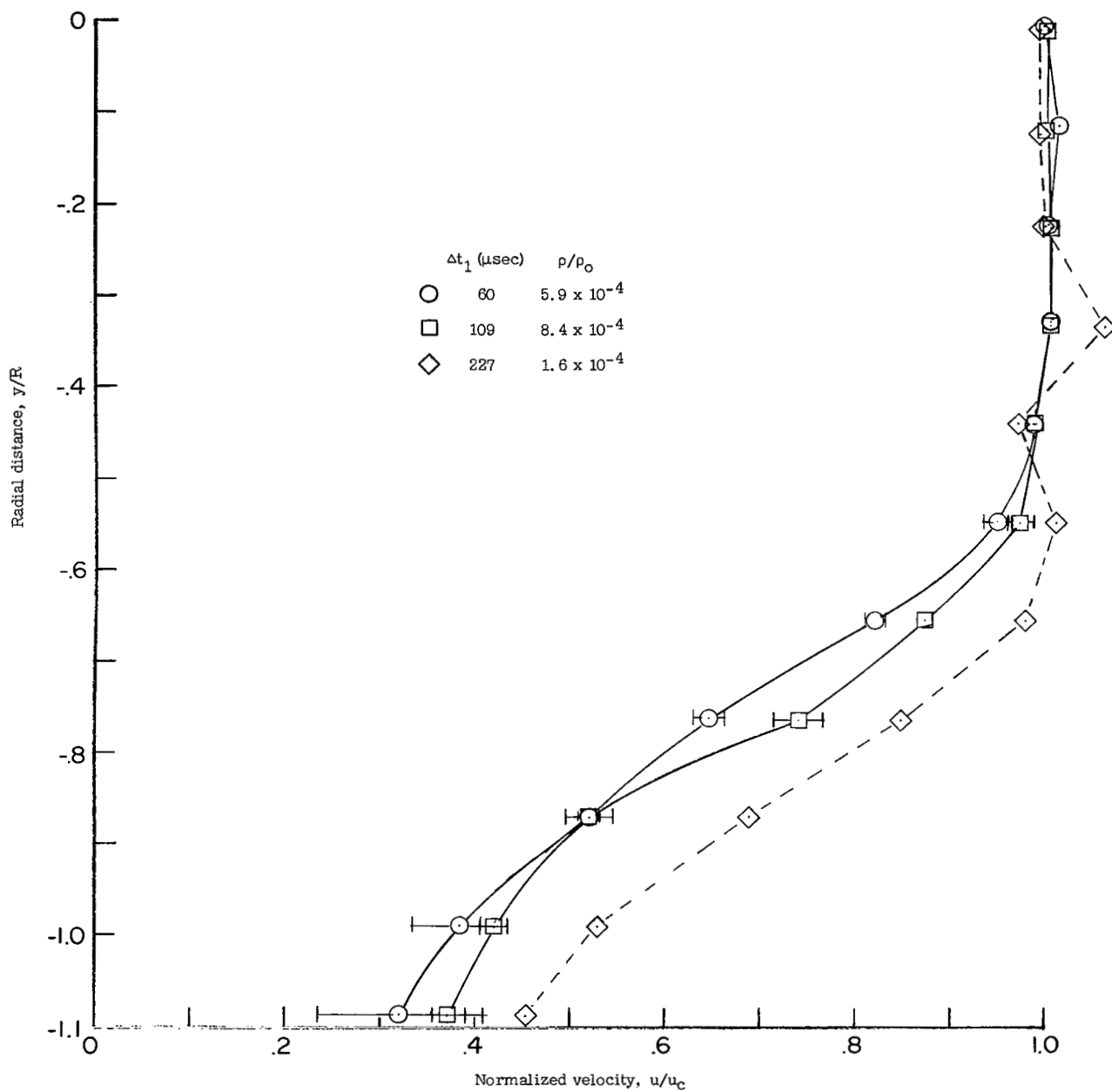
(a) $p_{10} = 0.01$ torr $= 1.3$ N/m^2; $p_1 = 22$ torr $= 2930$ N/m^2.

Figure 17.- Comparison of velocity profiles for various times behind He-air interface.

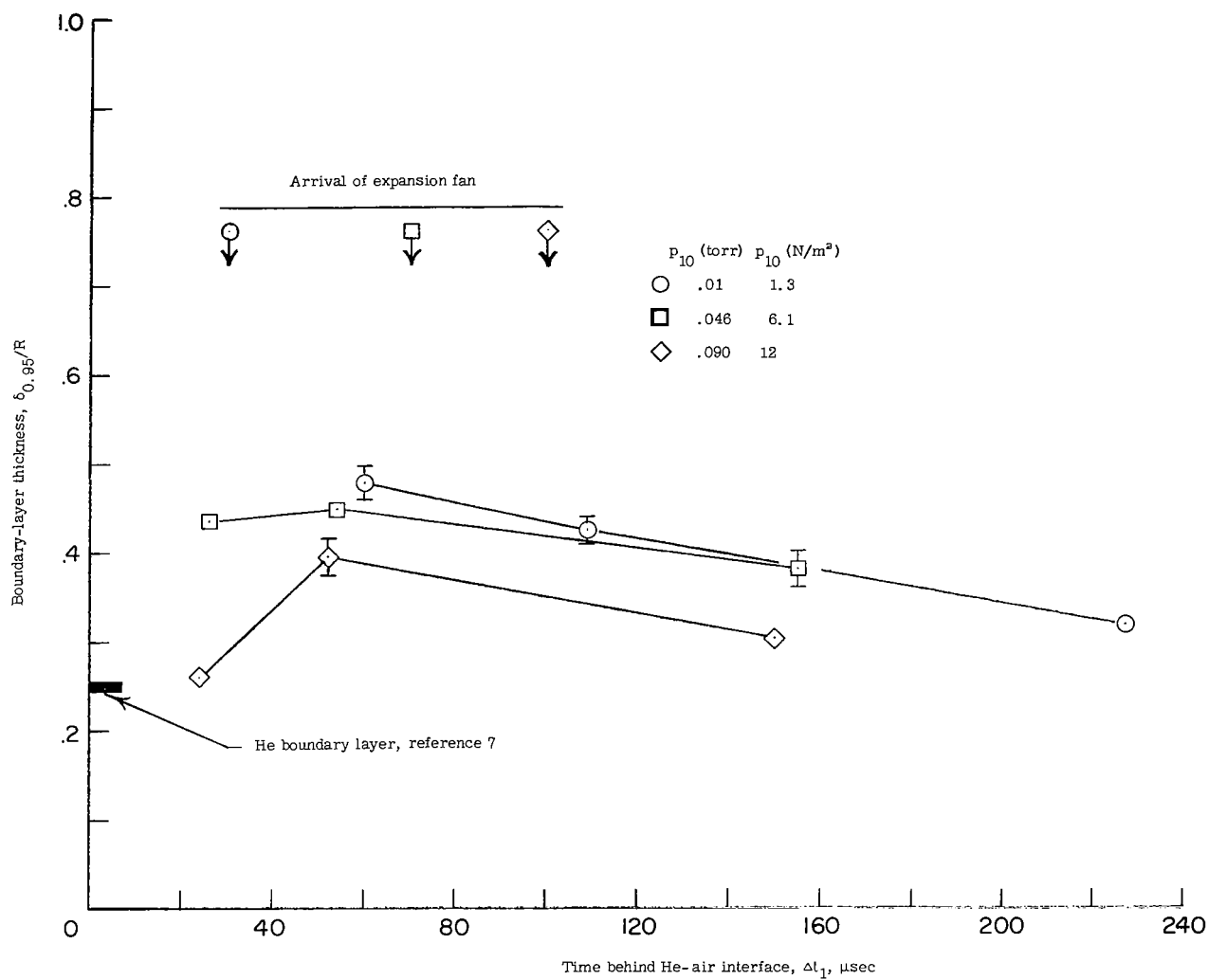(b) $p_{10} = 0.046$ torr $= 6.1$ N/m^2; $p_1 = 22$ torr $= 2930$ N/m^2.

Figure 17.- Continued.

Radial distance, y/R
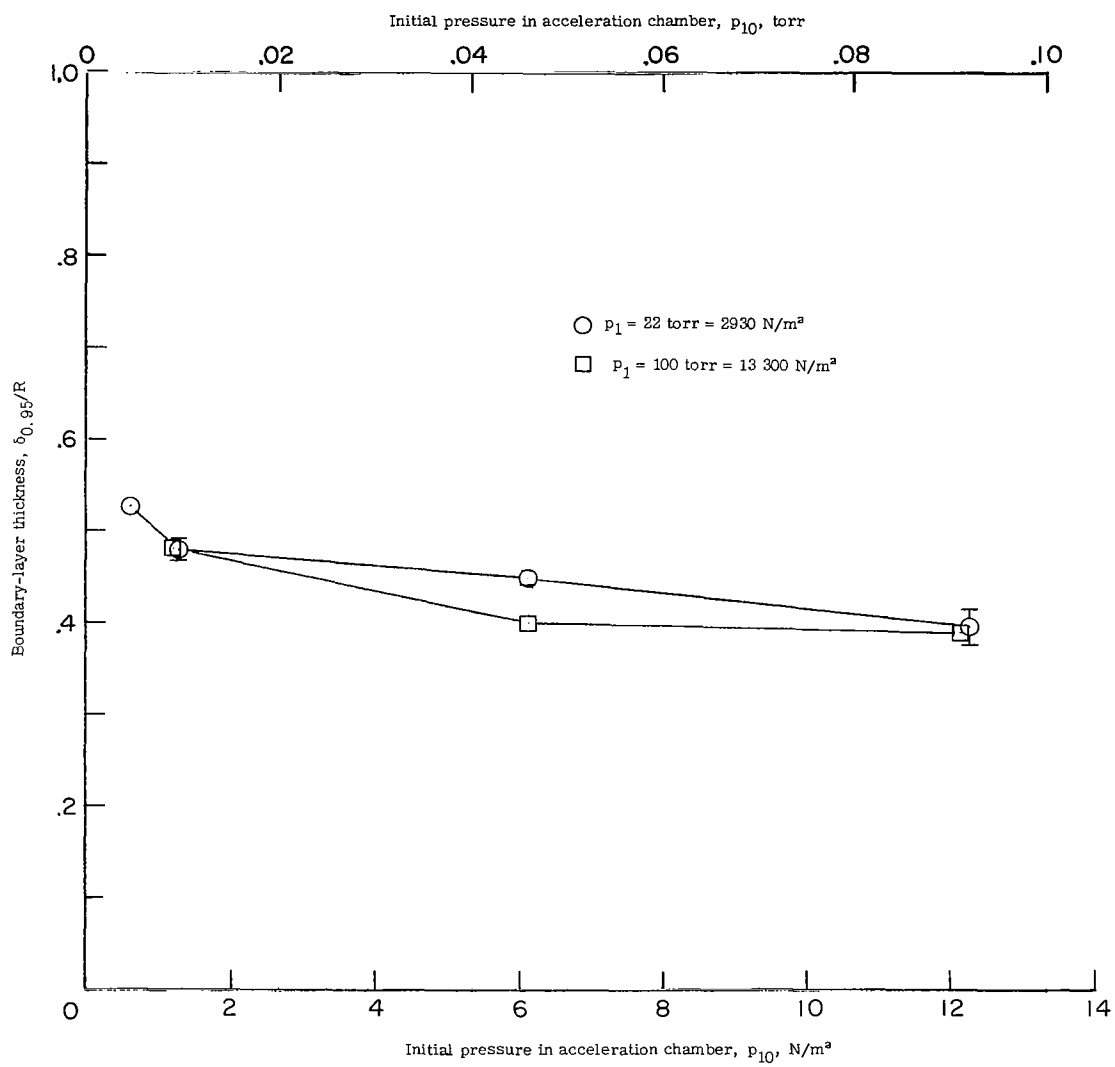
Δt_1 (μsec) ρ/ρ_0

O   24 1.8×10^{-3}
□   52 1.5×10^{-3}
◇   150 1.9×10^{-3}

0   .2   .4   .6   .8   1.0

Normalized velocity, u/u_c

(c) $p_{10} = 0.09$ torr $= 12$ N/m^2; $p_1 = 22$ torr $= 2930$ N/m^2.

Figure 17.- Concluded.

39

(a) $p_1 = 22$ torr $= 2930$ N/m^2.

Figure 18.- Variation of wall boundary-layer thickness.

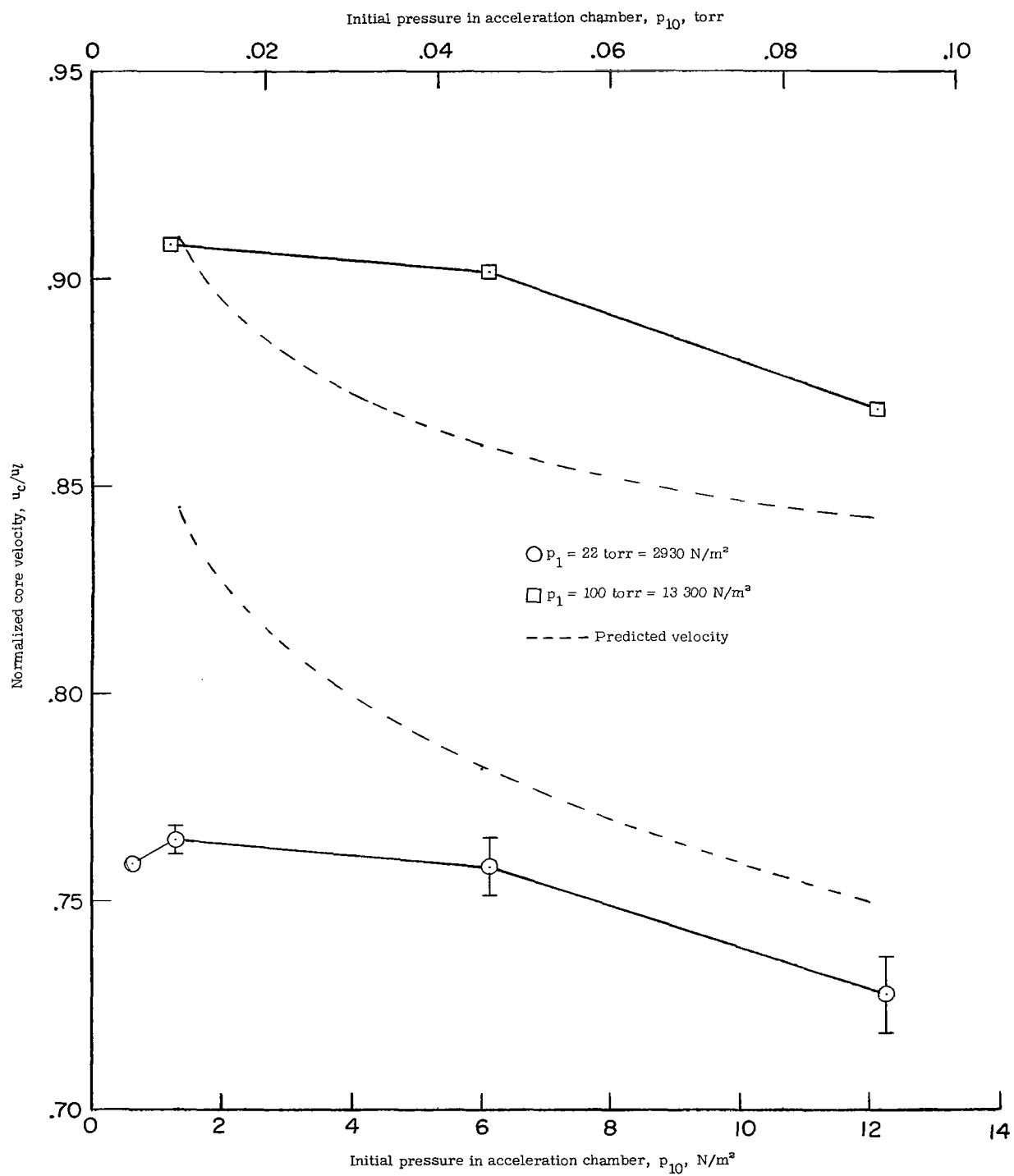Initial pressure in acceleration chamber, p_{10}, torr

Boundary-layer thickness, $\delta_{0.95}/R$

Initial pressure in acceleration chamber, p_{10}, N/m²

○ $p_1 = 22$ torr = 2930 N/m²

□ $p_1 = 100$ torr = 13 300 N/m²

(b) $\Delta t_1 = 52$ to 60 μsec.

Figure 18.- Concluded.
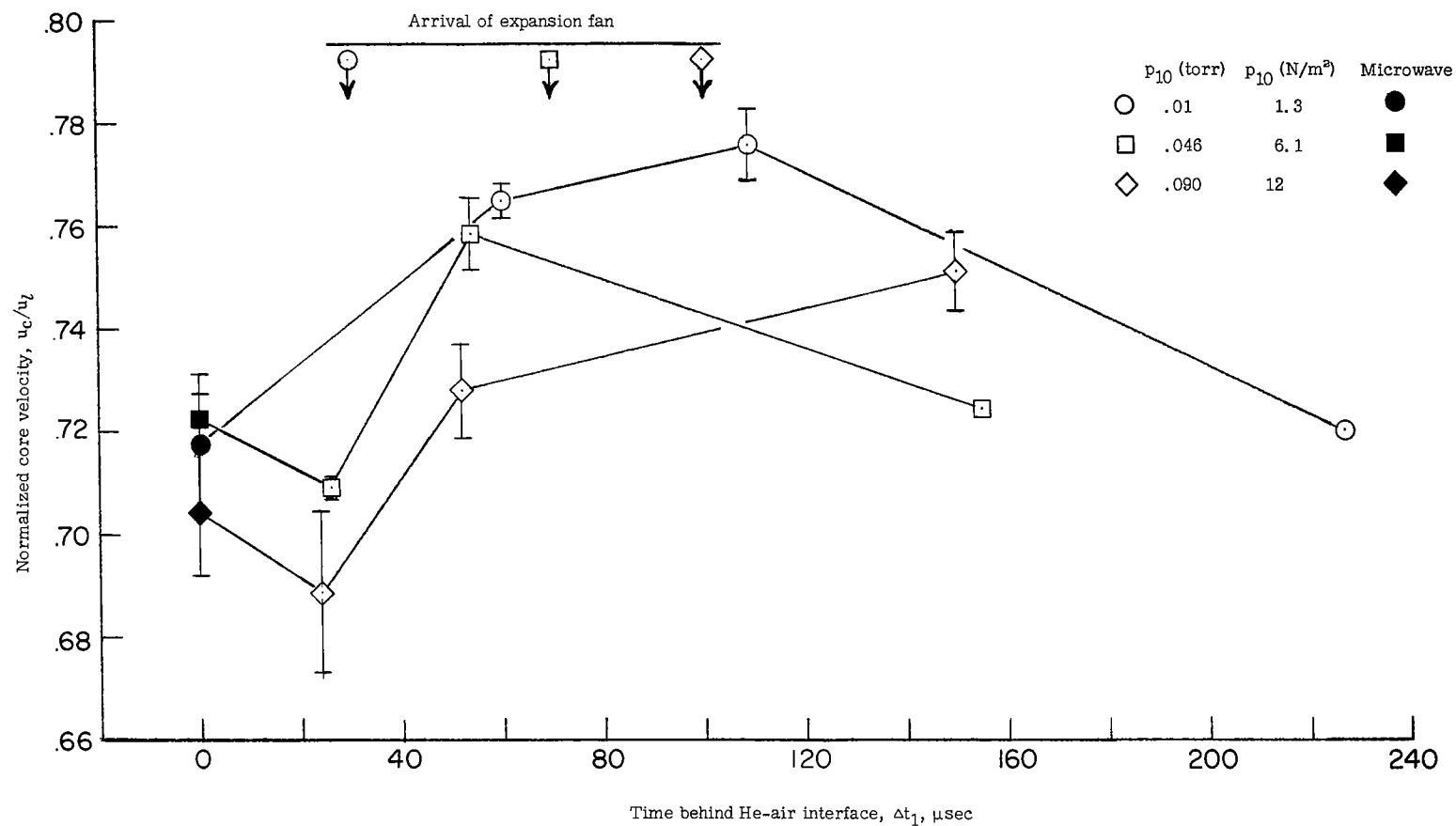
(a) $p_1 = 22$ torr $= 2930$ N/m^2.

Figure 19.- Variation of flow-core velocity.

Initial pressure in acceleration chamber, p_{10}, torr

Normalized core velocity, u_c/u_l

$\bigcirc\ p_1 = 22\ torr = 2930\ N/m^2$

$\square\ p_1 = 100\ torr = 13\ 300\ N/m^3$

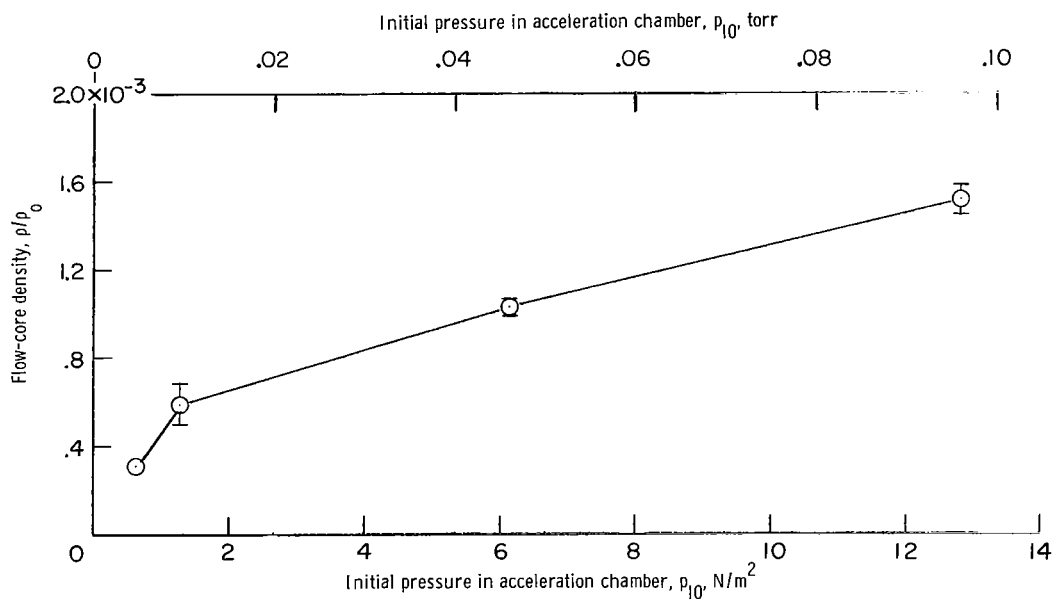$-\ -\ -\ $ Predicted velocity

Initial pressure in acceleration chamber, p_{10}, N/m^2

(b) $\Delta t_1 = 52$ to 60 μsec.

Figure 19.- Concluded.
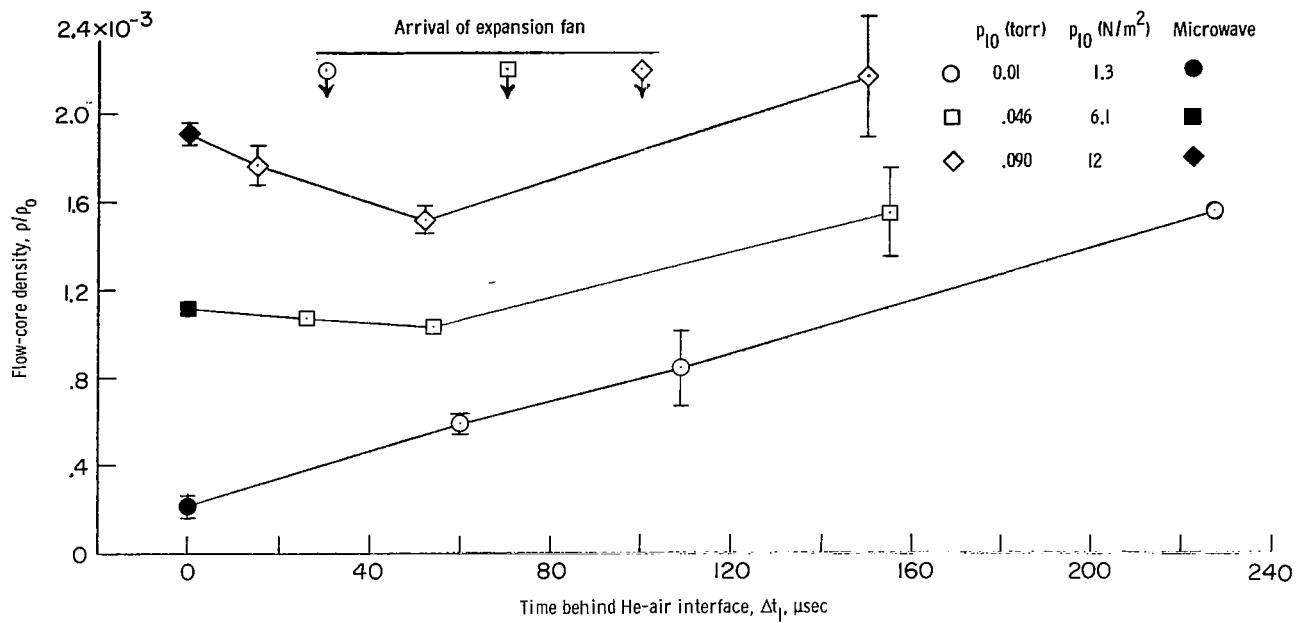
(a) p_1 = 22 torr = 2930 N/m^2.

(b) Δt_1 = 52 to 60 μsec; p_1 = 22 torr = 2930 N/m^2.

Figure 20.- Variation of flow-core density.